

## Chapter 2

# Introduction on High Intensity Laser-Plasma Interaction and High Field Plasmonics

This dissertation deals mainly with the attempt to extend the study of plasmonic effects in the ultra-high intensity (beyond  $10^{18}$  W/cm<sup>2</sup>) laser-matter interaction regime. Plasmonics, which is the study of surface plasmons, is a mature research field. However, surface plasmons are generally excited with low-intensity laser pulses. The study of plasmonic effects when ultra-high intensity lasers are involved is an almost completely unexplored ground. In this regime, which will be referred to as *High Field Plasmonics* in the following, relativistic, strongly non-linear effects are expected to take place.

This chapter is intended to provide a concise overview on laser-matter interaction in this intensity regime and to introduce the topic of High Field Plasmonics.

Section 2.1 provides an overview of high intensity laser technology. In Sect. 2.2 we give a brief introduction on the theory of laser-matter interaction in the high field regime, characterized by relativistic and strongly non-linear effects. Finally, Sect. 2.3 provides a synthetic theoretical introduction on what is meant for High Field Plasmonics, highlighting in particular possible future developments and foreseen difficulties.

## 2.1 Evolution of High Intensity Laser Technology

Since the realization of the first laser<sup>1</sup> in 1960 [3], laser technology underwent a tremendous development. An impressive and yet unbroken series of innovations has led to the realization of a wide variety of laser systems with very different features,

---

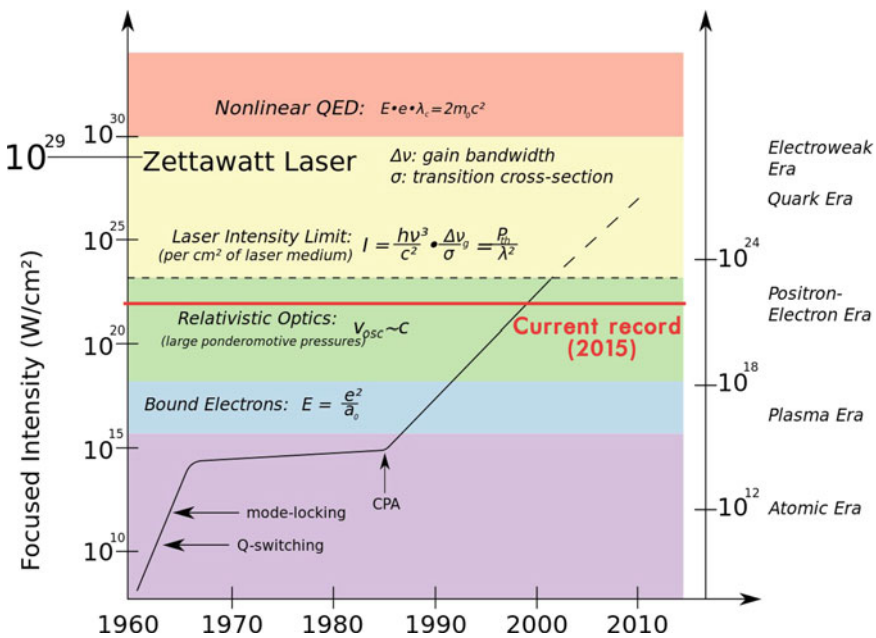
<sup>1</sup>The first Laser was preceded by the first Maser in 1953 [1], operating in the microwave region of the electromagnetic spectrum. Basic laser physics is beyond the scope of this dissertation and the interested reader is referred to [2].

enabling a broad range of applications [4], so that today the use of lasers is pervasive in both science and technology.

In this document, we take a very partial view on the history of lasers: the brief overview given in Sect. 2.1.1 will be limited to ultra-high intensity laser systems.

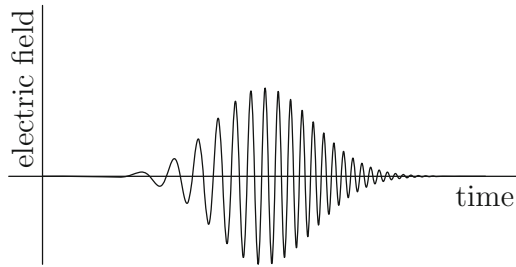
### 2.1.1 Overview

Figure 2.1 shows synthetically the development of high intensity laser systems over time. Starting from 1960, intensity increased at a fast pace for approximately a decade. This evolution was marked by two main innovations: Q-switching [7] and mode-locking [8]. These schemes allowed to increase the peak intensity of laser irradiation by orders of magnitude. Q-switching strategy is based on the sudden variation of the quality factor of the resonator cavity containing the laser active medium (this allows for more electrons to reach the excited state). The mode-locking strategy instead relies on the phase coherence of the cavity modes in the resonator. Both schemes result in a pulsed rather than a continuous emission.



**Fig. 2.1** In this graph, the maximum intensity reached by laser systems is shown as a function of time. The main innovations leading to higher intensities are highlighted. The red horizontal curve represents the current record (see [5]). The terminal part of the trend line (the black curve) is based on estimations formulated around 2000, which have proven to be over-optimistic. The picture was adapted from [6] (Color figure online)

**Fig. 2.2** This graph illustrates the electric field as a function of time for a chirped pulse. The instantaneous frequency of the pulse is evidently a function of time. In this case the instantaneous frequency grows linearly with time and the pulse is called *upchirped*



In order to reach high intensities, the laser emission of the resonator cavity can be fed into a sequence of amplifying stages. Indeed, if coherent radiation is made to pass through an excited active medium, it stimulates further coherent radiation emission. Thus a laser pulse can be coherently amplified extracting energy from the active medium.

Of course the possibility to reach extremely high intensities is strongly linked to the pulse duration. Presently the highest peak power of a laser system is of the order of 1 PW, which can be sustained at most for few ps or tens of ps (most PW class laser system have a pulse duration of only tens of fs).<sup>2</sup> The requirement on pulse duration is a strong limit for the active medium since the well known inequality  $\Delta\tau\Delta\omega \geq 1/2$  forces the active medium to operate in a large frequency range  $\Delta\omega$  (i.e. it should have a large *gain bandwidth*) in order to have a short  $\Delta\tau$ . Three main technologies are exploited for high intensity laser systems: Titanium:Sapphire [10] lasers (the active medium is a Sapphire,  $\text{Al}_2\text{O}_3$ , crystal doped with Titanium ions),  $\text{CO}_2$  lasers [11–13] (with a gaseous active medium containing  $\text{CO}_2$ ) and Nd:YAG lasers [10] (based on neodymium doped yttrium-aluminium garnet crystal). The shortest pulse durations which can be obtained with Nd:YAG lasers and  $\text{CO}_2$  lasers are, respectively, in the ps range and in the 100 fs range, whereas Ti:Sapphire lasers can provide pulses with durations down to  $\sim 10$  fs. The record peak powers for Nd:YAG and Ti:Sapphire systems are in the PW range, while  $\text{CO}_2$  lasers are approaching the 100 TW milestone. Here we will be mainly concerned with Ti:Sapphire laser systems, since for High Field Plasmonics very short pulse durations are needed.

Despite the rapid growth in the sixties, as shown in Fig. 2.1 the maximum focused intensity remained flat for decades, until mid-eighties, when *Chirped Pulse Amplification* (see [14]) opened the way for a new fast-pace increase of peak focused intensities of laser systems.

For long time further improvements of laser peak intensities were prevented by the material limits of the laser chain. Indeed, increasing the pulse intensity would have damaged the optical components. Moreover, the amplification process itself is inefficient for very short, intense pulses. Chirped Pulse Amplification (CPA) allowed to overcome these difficulties.

<sup>2</sup>For a comparison, the average electrical power produced on Earth is  $\sim 2\text{--}3$  TW [9]. Thus a PW class laser system is hundreds of times more powerful than the total electric output of the Earth.

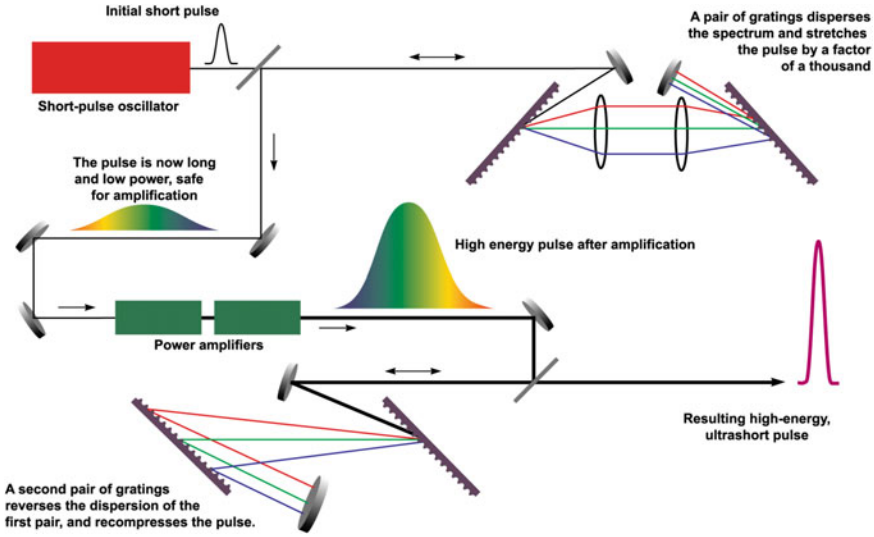


**Fig. 2.3** A typical implementation of CPA is shown. In this case the pulse stretching is obtained with a couple of gratings. After the first stage, the long chirped pulse is amplified through a series of power amplifiers. Finally the pulse is compressed again with a couple of gratings. These last gratings are typically very large, in order to avoid damage. This last stage of the optical chain is called *compressor*. The figure is reproduced from [15]

CPA consists essentially in increasing the temporal length of laser pulses introducing a chirp (see Fig. 2.2): spectral components of the pulse are dispersed in time according to their frequency (this *stretching* can be achieved with a couple of gratings or with a long optical fibre). A laser pulse whose spectral components are dispersed in time according to their frequency is called *chirped*.<sup>3</sup> A stretched pulse is easier to amplify efficiently and with lower damage risks for the optical components. Dispersion of spectral components can be reversed after the amplification stages with a couple of gratings in the *compressor* stage. In Fig. 2.3 a scheme of a typical CPA system is illustrated.

Currently, the record focused peak intensity for modern CPA-based laser systems is  $2 \times 10^{22} \text{ W/cm}^2$ , reached by a 300 TW Ti:Sapphire laser (see [5]).

### 2.1.2 A Typical High Intensity Ti:Sapphire Laser System

A typical High Intensity Ti:Sapphire laser system is roughly described by Fig. 2.3. An oscillator is responsible for producing a high-quality short pulse. These devices operate usually at a very high frequency ( $\sim \text{MHz}$ ), far beyond the capabilities of the

<sup>3</sup>An audio signal with similar properties recalls the chirping of birds.

other stages of the chain,<sup>4</sup> thus a single pulse is selected for further amplification. The pulse is then stretched and amplified in a sequence of stages. Typically, the active medium of these stages is efficiently *pumped* (i.e. excited) with other lasers, in order to prevent excessive heating. The amplified chirped pulse is finally compressed with a couple of gratings and sent to the interaction chamber, where the laser is focused on a target with a parabolic mirror.

Since several amplification stages are usually involved, care should be taken in order to avoid *gain narrowing*, which could increase pulse duration.

The laser pulse sent to the experimental room usually needs further optimizations. In particular, an inherent issue of high-power laser systems is the emission of intense prepulses both on the ns and the ps time scale before the main pulse. These pre-pulse, though sometimes useful, are typically detrimental for the experimental activity. Especially for High Field Plasmonics, for which the laser is made to interact with a solid structured target, a careful control of pre-pulses is needed. Control of pre-pulses is usually performed with plasma mirrors [16, 17]: the laser is focused on a transparent medium and the prepulses are either transmitted or absorbed. The plasma mirror is designed in such a way that a plasma is formed just before the main pulse, which is reflected with moderate losses. Most modern systems use a double plasma mirror. At the price of loosing  $\sim 50\%$  of the initial pulse energy, with a double plasma mirror a contrast of  $10^{10}$  can usually be achieved.

Finally, adaptive optics techniques are usually needed for focal spot optimization, in order to reach the highest possible focused intensities.

### 2.1.3 Towards 10 PW Laser Systems

Several projects to design and build ultra-intense laser systems able to overcome the PW limit are currently ongoing. A recent review on the current status and foreseen developments for ultra-high intensity laser technology can be found in [18]. PULSER laser at GIST (Gwangju, Republic of Korea) should soon operate in the multi-petawatt regime (4 PW are expected), since the upgrade from 1 PW is already in progress [19].

Apollon laser is being built in France with a target power of  $\sim 10$  PW [20]. Though the construction works have been delayed, also RAL-CLF facility (UK) has prepared plans for a 10 PW upgrade of Vulcan laser [21] and is currently involved in the validation of the concept. Both Apollon project and Vulcan upgrade project are based on on the Optical Parametric Chirped Pulse Amplification technique (OPCPA, see [22–24]).

Finally, in 2014, the large European project ELI (Extreme Light Infrastructure) has awarded a contract for the development and delivery of a 10 PW system to an industrial and academic consortium and also the Shanghai Institute of Optics and fine Mechanics (SIOM) is currently working on a 10 PW laser system [25].

---

<sup>4</sup>Ti:Sapphire laser systems operate in the 1–10 Hz frequency range (i.e. one shot every 0.1–1 s), mainly due to issues related to the amplifying stages.

If compared to the rapid development of high-intensity laser technology in the past decades, achieving the 10 PW milestone is requiring an amount of time significantly greater than expected. This might suggest that we are approaching the fundamental limits of current technology. However, some radically different schemes are currently being developed, though being still a concept at the moment. An example is the multi-fibre laser, whose development is currently pursued by the International Coherent Amplification Consortium. This laser system should consist in a large bundle of fibre-based lasers which are coherently combined to achieve extremely high intensities with a reasonable efficiency.<sup>5</sup> If the technical issues will be tackled, the proponents claim that this scheme could provide an efficient, high repetition rate 100 PW laser<sup>6</sup> concept (see [28, 29]).

## 2.2 Relativistic Laser Plasma Interaction

This section is intended to provide an introduction on Laser-Plasma interaction at ultra-high intensities. A natural starting point is single particle motion in a relativistic laser field. The study of ionization processes, which would be very important for lower laser intensities ( $I < 10^{16}$  W/cm<sup>2</sup>), is completely ignored here: at relativistic intensities, at least the outer electron shells of any atom are ionized within one laser cycle<sup>7</sup> [30]. Section 2.2.1 deals with single particle motion in intense laser fields. Electromagnetic (EM) waves propagation in a plasma is discussed in Sect. 2.2.2. Kinetic theory in the relativistic regime is briefly introduced in Sect. 2.2.3, whereas the importance of intense irradiation due to charged particle motion and QED effects at extremely high intensities are discussed in Sect. 2.2.6. Finally, possible applications and foreseen future developments of laser-plasma interaction are covered in Sect. 2.2.7.

The reader interested in Laser-Plasma interaction is referred to [30–32] which cover the topic extensively. For the Relativistic Kinetic theory a comprehensive reference is provided by [33].

### 2.2.1 Single Particle Motion

We start with a simple derivation of the non-relativistic *quiver motion* of an electron in an oscillating electric field. The equation of motion is simply:

---

<sup>5</sup>Fibre-based lasers can operate in the kW regime with a wall-plug efficiency  $\sim 30\%$ .

<sup>6</sup>Possible applications of a laser built according to this concept include space debris control [26] and production of Tc 99m [27], a radioactive isotope of medical interest.

<sup>7</sup>The critical intensity for ionization of any material with single photon processes is  $\sim 3.5 \times 10^{16}$  W/cm<sup>2</sup>.

$$\frac{d^2x}{dt^2} = -\frac{e_0}{m}E_0 \cos(\omega t) \quad (2.1)$$

We can integrate once Eq. 2.1, which leads to the following expression for the velocity as a function of time:

$$v = \frac{e_0 E_0}{m\omega} \sin(\omega t) \quad (2.2)$$

we define  $a_0$  as:

$$a_0 = \frac{v}{c} = \frac{e_0 E_0}{m\omega c} \quad (2.3)$$

The adimensional  $a_0$  parameter is crucial in Laser-Plasma interaction, since its value characterises the interaction properties:  $a_0 \ll 1$  means no relativistic effects,  $a_0 \lesssim 1$  is a regime with weakly relativistic effects,  $a_0 \geq 1$  defines the fully relativistic regime.

Equation 2.2 is oversimplified, since the effect of the magnetic field component is completely neglected. If  $v \ll c$  this approximation is justified: the strength of the force exerted by the magnetic field component is indeed suppressed by a factor  $v/c$ . However, if  $v \approx c$ , as in relativistic laser-plasma interaction, the magnetic and the electric field components become equally important. An exact solution of electron motion in an electromagnetic plane wave field can be found and the derivation is reported hereunder (closely following [30] and [31]).

The equations for particle momentum  $\mathbf{p}$  and energy  $E = m_e \gamma c^2$  read as follows:

$$\frac{d\mathbf{p}}{dt} = -e_0(\mathbf{E} + \frac{\mathbf{v}}{c} \times \mathbf{B}) \quad (2.4)$$

$$\frac{d}{dt} (m_e \gamma c^2) = -e_0 \mathbf{v} \cdot \mathbf{E} \quad (2.5)$$

with  $\mathbf{p} = \gamma m \mathbf{v}$  and  $\gamma = \sqrt{1 + p^2/m^2 c^2}$ .

We consider an elliptically polarized plane-wave, described by the vector potential  $\mathbf{A}$ , travelling along  $\hat{\mathbf{x}}$  ( $\mathbf{k} = k\hat{\mathbf{x}}$ ):

$$\mathbf{A}(\omega, \mathbf{k}) = (0, \delta a_0 \cos \phi, \sqrt{1 - \delta^2} a_0 \sin \phi) \quad (2.6)$$

where  $\phi = \omega t - kx$  is the phase. The  $\delta$  parameter controls the pulse polarization ( $\delta = 0, \pm 1$  means P-polarization, while  $\delta = \pm 1/\sqrt{2}$  means C-polarization).

Since  $\mathbf{E} = -\frac{1}{c} \partial_t \mathbf{A}$  and  $\mathbf{B} = \nabla \times \mathbf{A}$  (equal to  $\hat{\mathbf{x}} \times \partial_x \mathbf{A}$ ) we can re-write Eq. 2.4 as:

$$\frac{dp_x}{dt} = -e_0 \left( \partial_t \mathbf{A} + \frac{\mathbf{v}}{c} \times \nabla \times \mathbf{A} \right)_{|x} \quad (2.7)$$

$$\frac{d\mathbf{p}_\perp}{dt} = -e_0 \left( \partial_t \mathbf{A} + \frac{\mathbf{v}}{c} \times \nabla \times \mathbf{A} \right)_{|\perp} \quad (2.8)$$

where the momentum  $\mathbf{p}$  is broken down into its longitudinal and transversal compo-

nents. Using the fact that  $\mathbf{A} = \mathbf{A}_\perp$  (i.e.  $\mathbf{A}$  doesn't have a longitudinal component) and that  $\mathbf{v} \times \nabla \times \mathbf{A} = -v_x \partial_x \mathbf{A}_\perp$ , from Eq. 2.8 we get:

$$\frac{d}{dt} \left( \mathbf{p}_\perp - \frac{e}{c} \mathbf{A} \right) = 0 \quad (2.9)$$

which states the conservation of canonical momentum (related to translational invariance in the transverse plane).

It can be shown that a second conservation law can be written, replacing  $\mathbf{A}$  in Eq. 2.5:

$$\frac{d}{dt} (p_x - m_e \gamma c) = 0 \quad (2.10)$$

so that the particle motion is completely determined by the two constants of motion  $\mathbf{p}_\perp - \frac{e}{c} \mathbf{A}$  and  $p_x - m_e \gamma c$ .

Considering that the electron is initially at rest leads to the following solution, which depends parametrically on  $\delta$ :

$$\begin{cases} \frac{\hat{x}}{a_0^2} = \frac{1}{4} \left[ -\phi - \left( \delta^2 - \frac{1}{2} \right) \sin 2\phi \right] \\ \frac{\hat{y}}{a_0} = -\delta \sin(\phi) \\ \frac{\hat{z}}{a_0} = (1 - \delta^2)^{1/2} \cos(\phi) \end{cases} \quad (2.11)$$

where the coordinates have been normalized with respect to  $1/k$ . Figure 2.4 shows the trajectory of an electron in intense, P-polarized and C-polarized laser pulses. We immediately notice that in both cases there is a systematic drift of the electron along  $\hat{x}$ . It is evident from the graph that for P-polarization the electron is confined on the  $xy$  plane, while for C-polarization it spirals around the  $\hat{x}$  axis.

### 2.2.2 Propagation of EM Waves in a Plasma

After having derived the behaviour of a single electron in an intense oscillating EM field, the natural prosecution is the study of the propagation of EM waves in plasmas. For simplicity only the propagation of EM waves in cold, non-magnetized plasmas will be considered.<sup>8</sup>

The equation which describes the propagation of an EM wave reads as follows:

---

<sup>8</sup>The interested reader can find a thorough discussion of the rich physics of EM waves propagation in plasmas in [34].



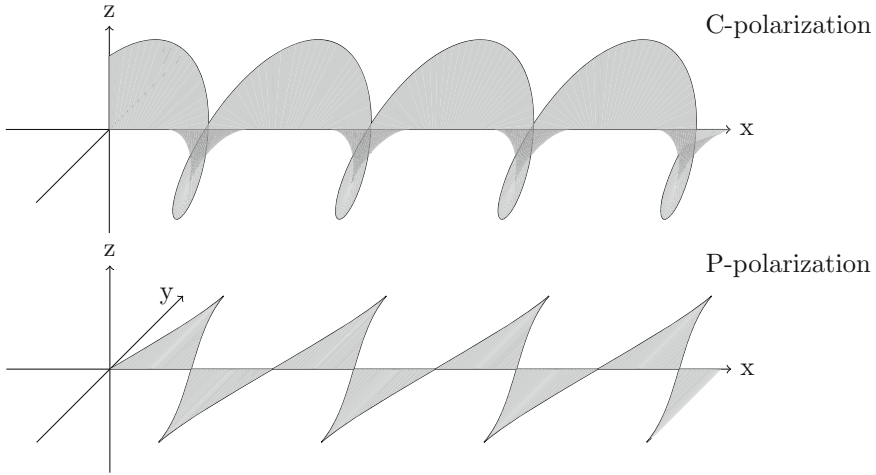


**Fig. 2.4** Trajectory of a charged particle under the effect of a relativistic C-polarized (upper panel) or P-polarized laser pulse

$$\left(\nabla^2 - \frac{1}{c^2} \partial_t^2\right) \mathbf{E} - \nabla(\nabla \cdot \mathbf{E}) = \frac{4\pi}{c^2} \partial_t \mathbf{J} \quad (2.12)$$

The derivation of the dispersion relation for EM waves in a cold plasma can be found in several standard textbooks [34, 35], thus only the result of the derivation will be reported here:

$$-k^2 c^2 + \epsilon(\omega) \omega^2 = 0 \quad (2.13)$$

where

$$\epsilon(\omega) = 1 - \frac{\omega_p^2}{\omega^2} \quad (2.14)$$

In the previous equation,  $\omega_p$  is the *plasma frequency*, defined as follows:

$$\omega_p = \sqrt{\frac{4\pi e^2 n_e}{m_e}} \quad (2.15)$$

Consequently, when  $\omega > \omega_p$  an EM wave is free to propagate in the plasma, whereas if  $\omega < \omega_p$  the EM wave is exponentially damped in the plasma. Given a fixed EM frequency  $\omega$  the *critical density*  $n_c$  is defined as the plasma density which makes  $\omega_p = \omega$ . For a laser wavelength  $\sim 800$  nanometers,<sup>9</sup> the critical density  $n_c \sim 2 \cdot 10^{22} \text{ cm}^{-3}$ .

The previous derivation is valid for a non-relativistic case. Relativistic laser-plasma interaction is significantly more challenging to study. Indeed, the strongly

<sup>9</sup>As for a typical Ti:Sapphire laser system.

non-linear effects lead to the complicated regime of non-linear optics.<sup>10</sup> However, at least for circularly polarized EM waves, an exact solution exists, provided that finite time and finite space effects are disregarded. In this last case the correct dispersion relation can be obtained with the replacement  $m_e \rightarrow \gamma_e m_e$ , where  $\gamma_e = \sqrt{1 + a_0^2/2}$ . This means that, in general, for a given frequency  $\omega$ , relativistic effects raise the critical density  $n_c$  to  $\gamma_e n_c$ . This phenomenon is called *relativistic transparency*.

### 2.2.3 Relativistic Kinetic Equations

In several physical scenarios, kinetic effects cannot be neglected. Here a synthetic derivation of relativistic kinetic equations is given (a comprehensive treatment can be found in [33]).

The relativistic one-particle distribution function  $f(x, p)$  is the probability of finding a particle within a small  $\Delta^4 x$  around four-position  $x$  and a small  $\Delta^4 p$  around four-momentum  $p$  (following reference [33], a classical picture is adopted, thus all quantum effects are neglected).

Given a collection of identical particles with mass  $m$ ,  $f(x, p)$  is defined as a statistical average of  $\sum_{i=1}^N \delta^3(\mathbf{x} - \mathbf{x}_i(t)) \delta^3(\mathbf{p} - \mathbf{p}_i(t))$ , where  $\mathbf{x}_i(t)$  and  $\mathbf{p}_i(t)$  are, respectively, the three-position and the three-momentum of particle  $i$  at time  $t$ <sup>11</sup>:

$$f(x, p) = \left\langle \sum_{i=1}^N \delta^3(\mathbf{x} - \mathbf{x}_i(t)) \delta^3(\mathbf{p} - \mathbf{p}_i(t)) \right\rangle \quad (2.16)$$

Using  $f(x, p)$ , particle four-flow density can be defined as:

$$N^\mu = c \int \frac{d^3 p}{p^0} f(x, p) \quad (2.17)$$

We will now derive the collisionless kinetic equation for the evolution of  $f(x, p)$  without any external force. We can define the scalar quantity  $\Delta N(x, p)$  as follows:

<sup>10</sup>Phenomena like self-focusing, higher frequency generation ... may take place and concepts like the refraction index and the dispersion relation cannot be ported straightforwardly in this regime.

<sup>11</sup>Though not manifestly covariant,  $f(x, p)$  can be proven to be a Lorentz scalar using the ancillary function  $\mathcal{N}(x, p) = \frac{1}{p^0} \delta(p^0 - \sqrt{p^2 + m^2 c^2}) f(x, p)$ . It is possible to show that  $\mathcal{N}(x, p) = \frac{1}{mc} \int d\tau \langle \sum_{i=1}^N \delta^4(x - x_i(t)) \delta^4(p - p_i(t)) \rangle$ , which is a Lorentz scalar ( $\tau$  is the proper time). Moreover, it is trivial to show that  $\theta(p^0) \delta(p^\mu p_\mu - m^2 c^2) = \frac{\delta(p^0 - \sqrt{p^2 + m^2 c^2})}{2p^0}$ . Finally, since using the previous result  $\mathcal{N}(x, p) = \theta(p^0) \delta(p^\mu p_\mu - m^2 c^2) f(x, p)$ , we can conclude that  $f(x, p)$  is a Lorentz scalar.

$$\Delta N(x, p) = \int_{\Delta^3 \sigma} \int_{\Delta^3 p} d^3 \sigma_\mu \frac{d^3 p}{p_0} p^\mu f(x, p) \quad (2.18)$$

where  $d^3 \sigma_\mu$  (time-like four-vector) is an oriented three-surface element of a plane space-like surface.  $\Delta N(x, p)$  can be interpreted as the number of world lines crossing the surface element  $\Delta^3 \sigma$  with a four-momentum within a volume  $\Delta^3 p$  centred on  $p^\mu$ .

After some time, the same number of world lines will cross the surface element  $\Delta^3 \hat{\sigma}$ . Thus we get:

$$\int_{\Delta^3 \hat{\sigma}} \int_{\Delta^3 p} d^3 \sigma_\mu \frac{d^3 p}{p_0} p^\mu f(x, p) - \int_{\Delta^3 \sigma} \int_{\Delta^3 p} d^3 \sigma_\mu \frac{d^3 p}{p_0} p^\mu f(x, p) = 0 \quad (2.19)$$

The bundle of word lines crossing  $\Delta^3 \sigma$  and  $\Delta^3 \hat{\sigma}$  defines a word line tube, whose enclosed four-volume is  $\Delta^4 x$ . Since there are no collisions, world lines cannot cross the borders of the tube. Exploiting Gauss theorem we can write

$$\int_{\Delta^4 x} \int_{\Delta^3 p} d^3 \sigma_\mu \frac{d^3 p}{p_0} p^\mu \partial_\mu f(x, p) = 0 \quad (2.20)$$

which immediately leads to

$$p^\mu \partial_\mu f(x, p) = 0 \quad (\partial_t + \mathbf{u} \cdot \nabla) f(x, p) \quad (2.21)$$

Equation 2.21 simply describe the free-streaming of the distribution function ( $\mathbf{u}$  is the three-velocity  $\mathbf{u} = \mathbf{p}/(\gamma m_0)$ ).

A very similar derivation can be carried out also if an external force  $F^\mu$  is present. In this case, a particle following a world line between  $\Delta^3 \sigma$  and  $\Delta^3 \hat{\sigma}$  changes momentum as follows:  $p^\mu \rightarrow p^\mu + F^\mu \Delta \tau$ , where  $\tau$  is the proper time.

Omitting the full derivation (details can be found in [33]), the final result for the relativistic kinetic equation is:

$$p^\mu \partial_\mu f(x, p) + m F^\mu \frac{\partial}{\partial p^\mu} f(x, p) = 0 \quad (2.22)$$

Equation 2.22 is valid only if  $F^\mu$  doesn't alter the rest mass  $m_0$  of the particles ( $p^\mu F_\mu = 0$ ) and if  $\frac{\partial F^\mu}{\partial p^\mu} = 0$ . It is worth to mention that these conditions are satisfied for the electromagnetic force  $F^\mu = -\frac{q}{mc} \mathcal{F}^{\mu\nu} p_\nu$  (where  $\mathcal{F}^{\mu\nu}$  is the electromagnetic tensor).

Equation 2.22 can be rewritten as

$$(\partial_t + \mathbf{u} \cdot \nabla + \mathbf{F} \cdot \frac{\partial}{\partial \mathbf{p}}) f(x, p) = 0 \quad (2.23)$$

### 2.2.4 Energy Absorption with Overdense Targets

In the previous subsection we have shown that an EM wave cannot penetrate in an overdense plasma. When fully ionized, solid density targets are strongly overdense ( $n_e/n_c \gg 100$ ) for Ti:Sapphire fs lasers. This means that a laser pulse is usually reflected from these targets, unless they are so thin that the laser is able to break through them.

Even if the laser is reflected back, a significant fraction of its energy may be transferred to the electrons of the target. Indeed “fast electrons” with energies of a few MeVs can usually be observed for ultra-high intensity laser-matter interaction. The typical order of magnitude of the hot electron energies as a function of the  $a_0$  parameter can be estimated<sup>12</sup> as  $E_{hot} = m_e c^2 \left( \sqrt{1 + a_0^2/2} - 1 \right)$ , so that laser-solid interaction with a  $a_0 = 5$  (typical for 100TW laser systems) the expected energy for the hot electron emission is  $\sim 1.4$  MeV. Depending on the irradiation conditions, several heating processes exist and the most relevant for ultra-high intensity laser interaction with solid density plasmas are listed below (see [31, 36] for a more detailed discussion). Electron heating is strongly dependent on the pulse parameters (polarization, angle of incidence, intensity) and on the target properties (density of the plasma, steep interface or smooth density gradient).

The study of electron heating processes is important because the expansion of the heated electrons leads to very intense electrostatic fields, which in turn can accelerate ions (see Sect. 2.2.7). Since high energy ion sources are of interest for several applications, understanding and controlling these processes may be beneficial for the optimization of laser-based ion sources.

#### Resonance Absorption

A possible mechanism for electron heating in laser-plasma interaction is *resonance absorption*, which can take place in a region of the plasma where the plasma frequency  $\omega_p$  is equal to the laser frequency  $\omega$ . Indeed, in these conditions, the laser can efficiently couple with the normal modes (bulk plasmons) of the plasma, which propagate with a frequency  $\omega_p$ . Of course, if a solid target is (even partially) ionized,  $\omega_p \gg \omega$ . However, intense laser pulses are frequently preceded by a less intense prepulse on the ps (or even ns) timescale. If the pre-pulse is sufficiently intense, it may lead to a pre-expansion of the target, forming a density gradient. The resonance absorption mechanism can then take place in the region of this plasma gradient in which the resonance condition is satisfied.

A simple electrostatic model of the process is described in [31] and is reported here.

The EM wave is described as an external oscillating field  $\mathbf{E} = \Re \left( \tilde{\mathbf{E}}_d e^{-i\omega t} \right)$ . The EM wave propagates in a plasma with a background density which is a function of the position  $n_0 = n_0(x)$ . The following system of equations can be written for this physical scenario, combining Gauss’s law for the electric field with fluid equations

<sup>12</sup>This estimated energy is called the “ponderomotive energy”.

for the plasma:

$$\begin{cases} \nabla \cdot \mathbf{E} &= -4\pi e(n_e - n_0) \\ \partial_t n_e &= -\nabla \cdot (n_e \mathbf{u}) \\ (\partial_t - \mathbf{u} \cdot \nabla) \mathbf{u} &= -\frac{e}{m_e} (\mathbf{E} + \mathbf{E}_d) \end{cases} \quad (2.24)$$

Linearising the previous equations in the limit  $u_x \ll L/\omega$  (i.e. density is considered to be uniform over the electron oscillation amplitude) we get:

$$\delta n_e = \frac{1}{4\pi e} \frac{(\mathbf{E} + \mathbf{E}_d) \cdot \nabla n_0}{n_0(x) - n_c} \quad (2.25)$$

Equation 2.25 indicates that there is a resonance when the plasma density is equal to the critical density, unless  $\mathbf{E} \cdot \nabla n_0 = 0$ . This means that P-polarization and oblique incidence are required. Actually, the previous derivation should be modified for oblique incidence (the laser pulse is reflected back at a density lower than  $n_c$ , possibly preventing the coupling with bulk plasmons). A detailed analysis of this effect is however beyond the scope of this section.

### Vacuum Heating

Vacuum heating is an electron absorption process which takes place in high intensity laser-plasma interaction when steep plasma gradients are involved. This mechanism was first proposed by Brunel [37]. Essentially the combined electric field of the incident pulse and the reflected pulse is responsible for dragging the electrons out of the target. After a half-oscillation, the electrons are injected in the target at high energy (the oscillation energy) and, since the EM field is evanescent in the overdense plasma, they are free to propagate further in the target. This mechanism should produce a high-energy electron bunch every laser cycle (the properties of these bunches can be studied as described in [38]).

A minimal 1D model of the process can be provided (see [31, 36, 39]), considering a step-like plasma with ion density  $n_i = n_0 \Theta(x)$  and an EM field  $E = E_e + E_d$ , where  $E_e$  is the electrostatic component and  $E_d$  is the oscillating external driver field  $E_d = E_0 \sin(\omega t)$  (only the  $\hat{x}$  component of the fields is considered).

Adopting a fluid description of the plasma, the following equations can be written:

$$\begin{cases} \partial_x E_e &= 4\pi\rho = 4\pi e [n_0 \Theta(x) - n_e] \\ \partial_t n_e &= -\partial_x (n_e v_x) \\ \frac{dv_x}{dt} (\partial_t + v_x \partial_x) v_x &= -\frac{e}{m_e} (E_e + E_d) \end{cases} \quad (2.26)$$

As described in [31], switching to Lagrangian variables ( $x = x_0 + \xi$ ,  $\tau = t$  and  $d\xi/dt = v_x$ ) leads to the following solution:

$$\xi = -x_0 + u_d (\sin(\omega t) - \sin(\omega t_0)) - \frac{u_d \cos \omega t_0}{1 - (\omega/\omega_p)^2} (t - t_0) + \frac{u_d \omega}{2} (t - t_0)^2 \sin(\omega t_0) \quad (x_0 + \xi < 0) \quad (2.27)$$

where  $u_d = e\tilde{E}_e/(m_e/\omega)$ . The last term of Eq. 2.27 shows that the electrons experience a secular acceleration (they enter the plasma with a velocity  $\approx u_d$ ). In the relativistic regime, a reasonable approximation of the kinetic energy of the re-entrant electrons is given by the ponderomotive energy. The third term of Eq. 2.27 instead shows that there is a resonance when  $\omega \sim \omega_p$ .

Vacuum heating relies crucially on longitudinal field components, which are absent for S-polarized laser pulses or for normal incidence.

It can be shown (see [30] for the detailed derivation) that a good estimation of the laser absorption efficiency with the vacuum heating process (in the limit  $\omega \ll \omega_p$ , far from the resonance) can be obtained solving the following implicit equation:

$$\eta = \frac{1 + \sqrt{1 - \eta}}{\pi a_0} \left[ \left( 1 + a_0^2 \sin^2 \theta (1 + \sqrt{1 - \eta})^2 \right)^{1/2} - 1 \right] \frac{\sin \theta}{\cos \theta} \quad (2.28)$$

where  $\eta$  is the absorption efficiency and  $\theta$  is the angle of incidence of the pulse. Equation 2.28 is obtained assuming that the energy of the re-entrant electrons is the ponderomotive energy and taking into account self-consistently the reduction of the amplitude of the accelerating field due to the absorption process. A few solutions of Eq. 2.28 are represented in Fig. 2.5. For small  $a_0$  the absorption efficiency peaks at grazing incidence, while for large  $a_0$  the model predicts  $\eta$  to reach 1 at smaller angles of incidence.

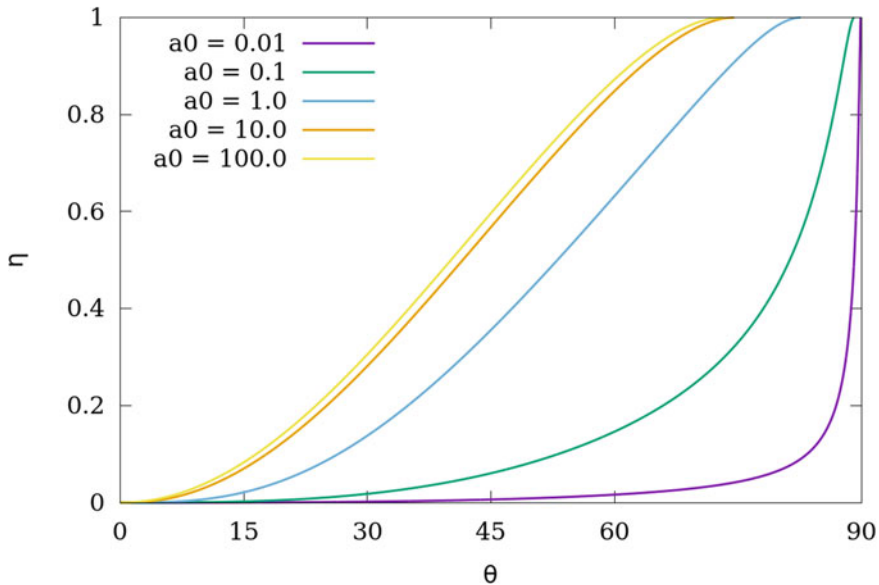


**Fig. 2.5** The solutions of Eq. 2.28 are shown for several  $a_0$ , ranging from  $a_0 = 0.01$  (non-relativistic regime) to  $a_0 = 100$  strongly relativistic regime

### **$\mathbf{J} \times \mathbf{B}$ Heating**

$\mathbf{J} \times \mathbf{B}$  heating mechanism [40] is similar to vacuum heating, since it requires a very steep plasma gradient. While in vacuum heating the electrons are extracted from the target and accelerated in the vacuum by the electric field of the pulse,  $\mathbf{J} \times \mathbf{B}$  relies on the  $\mathbf{v} \times \mathbf{B}$  term of the Lorentz force. At normal incidence,  $\mathbf{J} \times \mathbf{B}$  can be considered as a form of vacuum heating where  $E_d$  is replaced by  $\mathbf{v} \times \mathbf{B}/c$ . The main difference between the two processes is that  $E_d$  varies with a frequency  $\omega$ , while the frequency of  $\mathbf{v} \times \mathbf{B}/c$  is  $2\omega$ .

It can be shown that the longitudinal force exerted via  $\mathbf{J} \times \mathbf{B}$  mechanism is proportional to  $(1 - \cos(2\omega t))$ . The constant term is simply the ponderomotive force, while the oscillating term is responsible for accelerating electron bunches into the target with a frequency equal to  $2\omega$ . It can be shown that  $\mathbf{J} \times \mathbf{B}$  heating has a resonance for  $\omega = 2\omega_p$  (see [31]).

$\mathbf{J} \times \mathbf{B}$  heating applies for S and P polarization, also at normal incidence, while for C-polarization and normal incidence it can be shown that this mechanism is totally suppressed.

The absence of efficient electron heating mechanisms for C-polarization at normal incidence is exploited in ion acceleration schemes which rely solely on the radiation pressure on the target. In these schemes indeed, the generation of hot electrons is usually detrimental, since it may lead to an early disruption of the target.

### **2.2.5 Target Normal Sheath Acceleration (TNSA)**

In the previous subsection, it was mentioned that electron heating processes in solid density targets may lead to ion acceleration. Here, the most studied ion acceleration mechanism, TNSA (Target Normal Sheath Acceleration) is exposed in some detail. Other interesting ion acceleration schemes exist and they are briefly mentioned in Sect. 2.2.7. The interested reader is referred to [31, 36].

Ions are at least  $\sim 2000$  times heavier than electrons. Unless the laser pulse intensity exceeds  $10^{24} - 10^{25} \text{ W/cm}^2$  (far beyond what can be achieved with modern laser technology), the electric field of the pulse cannot accelerate directly the ions.

However, intense laser pulses can transfer a significant fraction of their energy to the electrons of the target, whose expansion leads to strong electrostatic fields. Ions can be accelerated up to high energies ( $\sim 60 \text{ MeV}$  at the moment) by these fields. The observation of these high energy ions dates back to the early 2000 (these experiments were performed with high energy “long” ns pulses, only recently experiments performed with fs Ti:Sapphire lasers have matched these results).

When an intense laser pulse interacts with a solid-density plasma, it transfers a significant fraction of its energy to a hot electron population. When hot electrons escape from the rear side of the target, they produce a sheath field  $E_s$  normal to the target surface. The magnitude of the sheath field can be estimated as  $E_s = \frac{T_h}{eL_s}$ ,

where  $T_h \sim m_e c^2 (\sqrt{1 + a_0^2/2} - 1)$  is the hot electron temperature,  $e$  is the elementary charge and  $L_s$  is the scalelength of the sheath field.  $L_s$  can be roughly approximated as  $L_s \sim L_D$ , where  $L_D = \sqrt{T_h/4\pi e^2 n_h}$  is the Debye length of the hot electrons.

Assuming a 10% laser absorption efficiency, a solid density plasma and a pulse intensity of  $\sim 10^{20} \text{ W cm}^{-2}$  the aforementioned estimations lead to a sheath field of  $\sim 6 \times 10^{10} \text{ V/cm}$ , which is orders of magnitude larger than what can be obtained in a conventional particle accelerator. Of course the sheath field decays rapidly after a few  $\mu\text{m}$ . Nonetheless, it is strong enough to ionize the impurities at the target surface (mainly carbon and hydrogen) and accelerate them up to a few tens of MeVs per nucleon. The acquired energy can be simply estimated as  $E \sim ZeE_s L_s$ , where  $Z$  is the atomic number of the ion. Replacing the formulae for  $E_s$  and  $L_s$  in the previous expression, we obtain a scaling law  $E \sim I^{1/2}$ , where  $I$  is the laser intensity. This is a rather unfavourable scaling, compared to other acceleration schemes like Radiation Pressure acceleration.

Reference [41] provides an extensive comparison of the theoretical models formulated for TNSA, concluding that the quasi-static approach [42] is particularly reliable to predict the energy of the accelerated ions.

### 2.2.6 Radiation Reaction Force and QED Effects

Laser-matter interaction with ultra-intense laser pulses leads to extreme electron acceleration, which become ultra-relativistic in a single laser-cycle. As widely known, an accelerated particle irradiates EM energy. The back-reaction force exerted on the particle due to this EM emission is called *Radiation Reaction* force (RR). Taking into account RR is important since it may significantly affect electron dynamics in laser matter interaction at intensities exceeding  $I \sim 10^{23} \text{ W/cm}^2$ , which will be available in the upcoming, next-generation laser facilities. Also the simulation of astrophysical scenarios involving ultra-relativistic plasmas may require RR to be considered.

RR can be considered as an additional term to the Lorentz fore:

$$\frac{d\mathbf{p}}{dt} = -e \left( \mathbf{E} + \frac{\mathbf{v}}{c} \times \mathbf{B} \right) + \mathbf{f}_{rad} \quad (2.29)$$

Considering the power dissipated by an accelerated charged particle:

$$P_{rad} = \frac{2e^2}{3c^3} |\dot{\mathbf{v}}|^2 = \frac{2e^2 \omega_c^2}{3c^3} \nu^2 \quad (2.30)$$

we may naively write an expression for  $\mathbf{f}_{rad}$ , so that  $\int_0^t \mathbf{f}_{rad} \cdot \mathbf{v} dt' = - \int_0^t P_{rad} dt'$ . This approach leads to



$$\mathbf{f}_{rad} = \frac{2e^2}{3c^3} \ddot{\mathbf{v}} \quad (2.31)$$

which is however unsatisfactory, since it allows runaway solutions.

In [43], the following expression for RR is derived:

$$\begin{aligned} \mathbf{f}_{rad} = & \frac{2r_c^2}{3} \left\{ -\gamma^2 \left[ \left( \mathbf{E} + \frac{\mathbf{v}}{c} \times \mathbf{B} \right)^2 - \left( \frac{\mathbf{v}}{c} \cdot \mathbf{E} \right)^2 \right] \frac{\mathbf{v}}{c} + \right. \\ & \left. + \left[ \left( \mathbf{E} + \frac{\mathbf{v}}{c} \times \mathbf{B} \right) \times \mathbf{B} + \left( \frac{\mathbf{v}}{c} \cdot \mathbf{E} \right) \mathbf{E} \right] - \gamma \frac{m_e c}{e} \left( \dot{\mathbf{E}} + \frac{\mathbf{v}}{c} \times \dot{\mathbf{B}} \right) \right\} \end{aligned} \quad (2.32)$$

where  $\dot{\mathbf{E}} = (\partial_t + \mathbf{v} \cdot \nabla) \mathbf{E}$  and  $\dot{\mathbf{B}} = (\partial_t + \mathbf{v} \cdot \nabla) \mathbf{B}$ . The expression for RR of Eq. 2.32 does not lead to runaway solutions.

A simple and effective numerical technique to include RR effects in PIC codes is presented in [44]. Despite its simplicity, this approach is able to reproduce the exact solution of Eq. 2.29 (obtained with expression 2.32 for  $f_{rad}$  [45]).

The description given for RR is completely classical. This means that this treatment is not valid when the laser field approaches the *Schwinger limit* in the reference frame co-moving with the electron:

$$E_s = \frac{m_e c^2}{\lambda_c} = 1.3 \times 10^{16} \text{ V cm}^{-1} \quad (2.33)$$

In this regime the electric field becomes high enough to generate electron-positron pairs from the vacuum. In the laboratory frame, the *Schwinger limit* corresponds to a laser intensity of  $\sim 10^{29} \text{ W/cm}^2$  (for Ti:Sapphire lasers), which is extremely higher than what can be achieved with present and foreseen laser technology. However, in the reference frame co-moving with the electron, the electric field is up-shifted by a factor  $2\gamma$ . This means that, in specific conditions, the onset of QED effects in laser-plasma interactions may be observed at much lower intensities [46].

## 2.2.7 Applications

In this section a condensed summary of the main trends in intense laser-plasma interaction research is given. An exhaustive treatment of these topics is far beyond the scope of this document. The following list is provided in order to account for the variety of this research field.

### Electron Acceleration

Electron acceleration is a long-standing topic in intense laser-plasma interaction. The idea of exploiting a laser-induced wake in an under-dense plasma for electron acceleration dates back to 1979 [47]. This scheme is known as *Laser WakeField Acceleration (LWFA)*

For Ti:Sapphire laser systems, targets with  $n < n_c$  are normally in gaseous form (gas jets synchronized with the laser pulse are used). Essentially, with a laser pulse propagating in a sub-critical plasma it is possible to induce periodic perturbations of the electron densities (this is due to the ponderomotive force). These density perturbations (see Fig. 2.6) are associated with a longitudinal electric field. Some electrons (coming from the plasma or externally injected) can be trapped inside the lower density region and, under the right conditions, they can be accelerated up to very high energies. Several different strategies have been explored in this field and in 2004 electron energies of  $\sim 200$  MeV (see [48]) were reached, while the current record is in the multi-GeV range (see [49]). The most attractive features of these plasma based accelerators are the extreme compactness of the source (the acceleration takes place in a few millimetres of plasma) and the very high intensity of the accelerated electron bunch (this is due to the fact that the bunch is extremely short in time, few 10s fs). Due to these properties, LWFA is also attractive as a secondary source of radiation.

A significant research effort in this field is currently focused on multi-stage LWFA accelerators [50], in which an electron bunch generated with LWFA is injected in another laser-driven wakefield. The final goal of this research line is achieving performances comparable with conventional accelerators (tens or hundreds of stages are thought to be required for this purpose).

Recently, approaches able to exploit the foreseen advancements in laser technology have been proposed (e.g. multi-fibre lasers), like plasma wakefield accelerators driven by an incoherent combination of laser pulses [51].

It is worth to mention here that, though not based on a laser driven wakefield, plasma wakefield accelerators (PWFA) have been tested successfully to boost the energy of electron bunches accelerated by a conventional Linac (see [52] for a recent result). The main idea behind PWFA is very similar to LWFA, except that the wakefield is generated by the electron bunch itself.

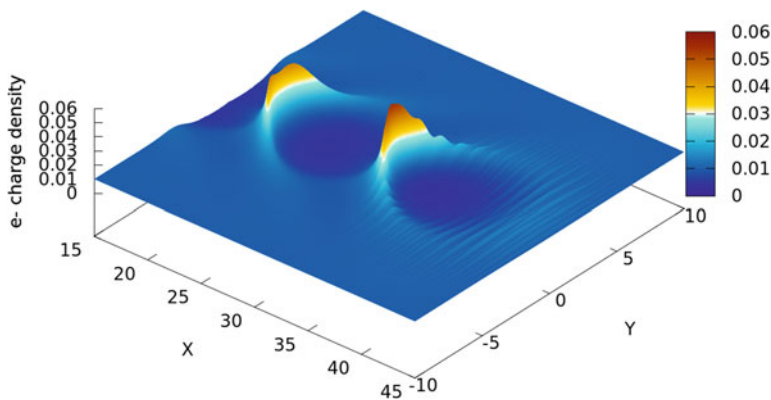


**Fig. 2.6** Laser WakeField Acceleration. Laser induced electron density perturbations are clearly visible. Strong longitudinal electric fields are associated with these perturbations

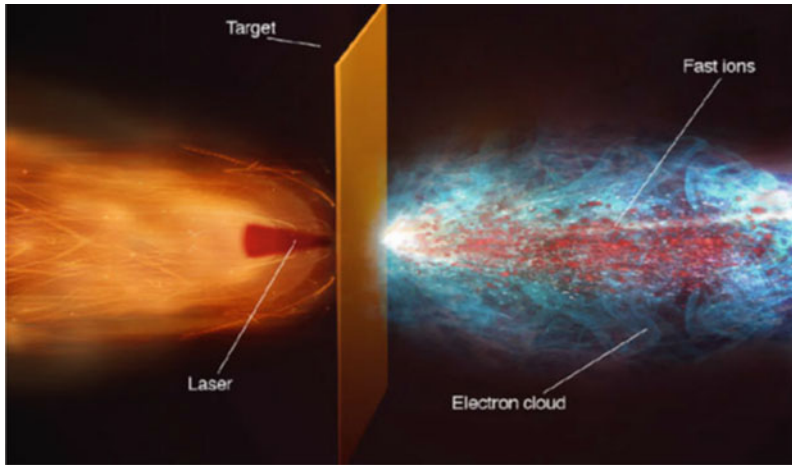


**Fig. 2.7** Target Normal Sheath Acceleration principle. Reprinted figure with permission from A. Macchi, M. Borghesi, and M. Passoni, *Reviews of Modern Physics* 85, 751 [36]. Copyright 2013 by the American Physical Society

### **Ion Acceleration**

Besides electrons, also ions can be accelerated by means of laser plasma interaction (see [36, 53] for a review). Normally, solid targets are used in this research field. The interaction of the laser pulse with solid targets results in the generation of a very high density plasma (typically  $\sim 300 n_c$ ).

Ions are too heavy to be accelerated directly by the laser pulse (even for the laser systems which will come online in the next years). Thus their acceleration is essentially due to the electrostatic field generated by the electrons. In a typical scenario, the so-called Target Normal Sheath Acceleration (TNSA), thin solid targets are used. The interaction of the laser pulse at the target surface generates a population of hot electrons. These electrons are expelled from the target, generating a very intense longitudinal electrostatic field at the back side. This electric field in turn accelerates the ions coming from the back side of the target<sup>13</sup> (see Fig. 2.7 for an artistic representation).

Several other ion acceleration schemes exist. Some are variations of the TNSA scheme which use structured targets to improve hot electron generation (coupled foam-solid targets or targets with a micro-structured surface). This topic will be covered extensively in Chap. 5.

Other schemes, such as Radiation Pressure Acceleration (RPA), differ significantly from the TNSA picture. In RPA, indeed, electron heating is suppressed and a charge separation is directly induced by the radiation pressure exerted on the electrons of the target (see Chap. 6).

Normally ion acceleration schemes are able to accelerate ions up to a few tens of MeV per nucleon. As for electron accelerators, laser-based ion acceleration schemes

<sup>13</sup>Normally a layer of hydrocarbon contaminants is always present on the target surfaces.

are interesting for their compactness. Moreover, if significant improvements over present laser plasma accelerators were achieved, they could become attractive for medical purposes. In fact, ions in the energy range of 100s MeV are routinely used for cancer treatment in several medical facilities in the world (the technique is called *hadron-therapy*). Ions are useful for cancer treatment because they release most of their energy at the Bragg peak. This means that it is possible to carefully select the ion energy in order to maximize the tissue damage on the cancer region, sparing the healthy tissues.

Medical facilities able to treat cancer with hadron-therapy use traditional accelerators (which are very expensive and require very large facilities). However, before plasma based accelerators could compete with traditional accelerators in this field, several important improvements should be achieved. In particular, laser-accelerated ions exhibit a cut-off energy which is still too low to be of medical interest. Moreover, their spectrum is extremely broad, while a quasi mono-energetic spectrum would be required. Finally, reliability of these plasma based systems should be improved.

Besides the medical use envisaged for laser-based ion sources, other interesting applications in material science may significantly relax the requirements for the accelerated ions. Indeed, present laser-based ion acceleration schemes may be already suitable or not too far from being suitable for some of these applications. This topic will be discussed in more detail in Chap. 5.

### High Harmonic Generation

High Harmonic Generation (HHG) (see [54]) is a vibrant research field, stemmed from the study of laser-matter interaction. Irradiating a gaseous target with relatively intense ultra-short laser pulses results in the generation of high-order harmonics. The semi-classical *recollision* model [55] is helpful to get an insight of the process. In the intense laser field, an electron can tunnel through the atomic potential into the vacuum, where it can be accelerated by the laser. After a half optical cycle the laser is reversed and the electron can recombine with its parent atom, emitting a burst of radiation.

The most attractive feature of HHG is the possibility to tune the process to generate extremely short laser pulses, down to the attosecond timescale [56], which are very attractive as a diagnostic tool for ultra-fast electronic processes in atoms and molecules.

In order to generate high-order harmonics and then attosecond pulses with gaseous targets, the intensity of the laser pulse cannot be greater than  $\sim 10^{16}$  W/cm<sup>2</sup>, which prevents the generation of *high intensity* attosecond pulses (the maximum energy of an intense attosecond pulse is  $\sim 1$   $\mu$ J [57]). A possible route to higher-intensity attosecond pulse sources consists in using overdense plasma surfaces and ultra-high intensity laser pulses [58, 59]. There are currently ongoing efforts to optimize harmonic generation with this scheme and to produce and isolate attosecond pulses. The topic will be covered more extensively in Chap. 6.

### Intense Gamma Sources

Electrons accelerated via the LWFA process may be exploited as a secondary source of radiation. Schemes based on Thomson scattering may be implemented to obtain compact and intense x-rays/gamma sources (see for example [60]).

Recently, a laser-based  $\gamma$  source set the record for the highest peak brilliance in the multi-MeV energy range:  $\sim 2 \times 10^{20}$  photons  $\text{s}^{-1}\text{mm}^{-2}\text{mrad}^{-2}$  (see [61]). This value exceeds by several orders of magnitude the peak brilliance that can be obtained with conventional sources available in that energy range.

### Laser-Based Neutron Sources

Laser-based particle acceleration (both of electrons and ions) opens interesting perspectives for compact, ultra-intense and ultra-short laser-based neutron sources.

Two mechanisms can be exploited: laser-based electron acceleration for photoneutron generation and nuclear reactions induced by laser-accelerated ions. As far as the first mechanism is of concern, Bremsstrahlung photons are generated with electrons in the multi-MeV or 10s MeV energy range interacting with a suitable solid target. The energy spectrum of these photons extends up to the initial electron energy [62] and it is thus suitable for photoneutron generation. Laser-based sources of photoneutrons were described in the past [63] and recently a few experiments have reported very high intensity neutron fluxes, exceeding several other bright neutron sources [64–66]. As far as the second mechanism is of concern, a “traditional” laser based ion acceleration scheme is coupled with a suitable target for neutron generation (see [66]).

As pointed out in [64], such short and intense pulsed neutron sources may have significant applications for the Fast Neutron Resonance Radiography technique [67] (which is useful for active material interrogation [68–71]). Moreover neutron sources based on laser systems foreseen in the near future may even allow to study nucleosynthesis processes in extreme astrophysical scenarios [72].

### Laboratory Astrophysics

The availability of high intensity laser sources allows to test mechanisms relevant for astrophysics in a laboratory environment (the so-called *laboratory astrophysics*). This allows to study physical scenarios which otherwise would be beyond reach for direct experimental testing. Several questions concerning crucial astrophysical processes are indeed still open and the research effort on this topic may take advantage from experimental tests. Scaling the parameters of astrophysical plasmas down to the laboratory scale can be done rigorously (see [73]). Typical laboratory astrophysics experiments involve the study of shocks and/or counter-streaming plasmas (see [74]).

Recently the generation of neutral and high-density electron-positron pair plasmas in the laboratory was demonstrated [75] and numerical studies [76] indicate that upcoming laser facilities will be able to provide pair plasmas with parameters suitable to test astrophysical scenarios.

Finally, energetic ns beams were used in the past to compress matter much beyond what can be achieved with diamond anvils (see [77] for an example): NIF facility (USA) was recently able to reach a pressure of  $\sim 1$  Gbar [78]. These studies are useful to understand the properties (crystalline structure, conductivity ...) of matter in

conditions analogous to those found in planetary cores. Recent results with nano-structured targets [79] suggest that extremely high pressures suitable for High Energy Density physics studies can be achieved even with ultra-high intensity fs lasers.

### **Laser-Plasma Interaction at Extreme Laser Intensities**

The advent of future laser facilities should allow to the observation of physical processes at energy scales beyond those of atomic physics (see [80] for a thorough review). For instance, laser intensities exceeding  $10^{23}$  W/cm<sup>2</sup> should be high enough to observe an electron dynamics strongly dominated by RR. Even higher intensities may allow in the future to test QED phenomena such as QED cascades and vacuum polarization.

## **2.3 High Field Plasmonics**

The excitation and control of Surface Plasmons (SPs) is a vibrant research field [81, 82], with several present and foreseen applications, ranging from extreme light concentration beyond diffraction limit [83] to biosensors [84] and plasmonic chips [85].

SPs are collective excitations of the electrons at the interface between a metal and a dielectric. “Classical” plasmonics schemes involve the interaction of low intensity ( $I < 10^{12}$  W/cm<sup>2</sup>) laser pulses with sub-wavelength structured targets (target structuring is required for SP excitation).

Some configurations of classical plasmonics may be extended into the high intensity laser-matter interaction regime. Plasmonics in this regime, where strongly non-linear effects are expected, is essentially unexplored.<sup>14</sup> SP excitation at relativistic intensities poses new questions and might open new frontiers for manipulation and amplification of high power laser pulses.

Section 2.3.1 provides an introduction on SP physics with an eye towards high field regime. An overview of classical plasmonics schemes is provided in Sect. 2.3.2, while in Sect. 2.3.3 the outlook for the research on high field plasmonics is discussed.

### **2.3.1 Excitation of Surface Plasmons**

In this section, only an introductory theoretical background on SP will be given. For a thorough treatment the interested reader is referred to [87, 88] (see instead [89] for a discussion on High Field Plasmonics).

SPs are electron oscillation modes which are confined at a steep interface between a metal and a dielectric material. We will first derive their dispersion relation before discussing their properties and how they can be excited.

---

<sup>14</sup>The excitation of surface waves in relativistic laser-matter interaction was first proposed in [86] but the topic has remained essentially unexplored up to now.

In a wide range of frequencies (far from the absorption regions and neglecting damping), the dielectric function of a metal can be approximated with the dielectric function of a plasma:  $\epsilon_r(\omega) = 1 - \omega_p^2/\omega^2$ , where  $\omega_p$  is the plasma frequency. We will consider a perfectly flat interface between a metal ( $\epsilon_2 = \epsilon_r(\omega)$ ) and a generic dielectric medium, characterized by the dielectric constant  $\epsilon_1$ . We will adopt the reference frame of Fig. 2.8:  $\hat{x}$  is perpendicular to the surface, while  $\hat{y}$  is the direction of propagation along the interface. The system is taken to be invariant along  $\hat{z}$ . Throughout the derivation subscripts 1 and 2 will be used to indicate, respectively, a field in the dielectric region ( $x > 0$ ) or in the metal region ( $x < 0$ ).

Given the system of Fig. 2.8, the following conditions for the EM field should be imposed:

$$\begin{cases} \mathbf{E}_{\parallel 1} = \mathbf{E}_{\parallel 2} \\ \mathbf{B}_{\parallel 1} = \mathbf{B}_{\parallel 2} \\ \epsilon_1 \mathbf{E}_{\perp 1} = \epsilon_2 \mathbf{E}_{\perp 2} \\ \mathbf{B}_{\perp 1} = \mathbf{B}_{\perp 2} \end{cases} \quad (2.34)$$

Subscripts  $\perp$  and  $\parallel$  indicate, respectively, the field component perpendicular to the surface and the field components parallel to the surface. It can be shown that no transverse electric modes (TE) can exist with these conditions (see [88]). We thus consider a transverse magnetic (TM) mode, for which we make the following ansatz (monochromatic SP):

$$\begin{cases} \mathbf{B} = B_0 \hat{z} e^{-qx} e^{i(ky - \omega t)} \\ \mathbf{E} = (E_{0x} \hat{x} + E_{0y} \hat{y}) e^{-qx} e^{i(ky - \omega t)} \end{cases} \quad (2.35)$$

where  $q$  may be different in the two regions.

Using  $\nabla \times \mathbf{B} = \mu \left( \frac{4\pi}{c} \mathbf{J} + \frac{\epsilon}{c} \frac{\partial \mathbf{E}}{\partial t} \right)$  and performing a Fourier transform with respect to time we get  $\nabla \times \tilde{\mathbf{B}} = -i\omega \epsilon \tilde{\mathbf{E}}/c$  (no current, magnetic permeability  $\mu \sim 1$ ).

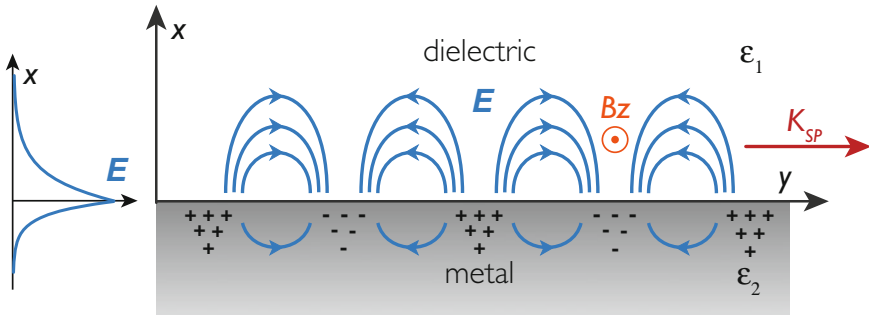


**Fig. 2.8** Schematic representation of the surface oscillation mode of the electrons at the steep metal-dielectric interface. The figure is reproduced with permission from [89]

If we insert the ansatz in Eq. 2.35 we finally get:

$$\tilde{\mathbf{E}} = \frac{-c}{\omega\epsilon} [k\hat{\mathbf{x}} - iq\hat{\mathbf{y}}] B_0 \quad (2.36)$$

Imposing the boundary conditions of Eq. 2.34 we find:

$$\frac{q_1}{\epsilon_1} = \frac{q_2}{\epsilon_2} \quad (2.37)$$

Since we are looking for solutions bounded to the interface,  $q_1$  and  $q_2$  should be real and with opposite sign ( $q_1$  should be positive,  $q_2$  should be negative in order to avoid divergences at  $x = \pm\infty$ ). This is only possible if  $\epsilon_1$  and  $\epsilon_2$  have opposite sign (i.e. if one medium is a dielectric and the other one is a metal).

In general, in a medium with dielectric function  $\epsilon(\omega)$ , the magnetic field  $\mathbf{B}$  satisfies Helmholtz equation  $\left(\nabla^2 + \epsilon \frac{\omega^2}{c^2}\right) \mathbf{B} = 0$ . This implies:

$$q^2 - k^2 + \frac{\omega^2}{c^2} \epsilon = 0 \quad (2.38)$$

Since  $k$  should be the same for the metal region and the dielectric region:

$$q_1^2 + \frac{\omega^2}{c^2} \epsilon_1 = q_2^2 + \frac{\omega^2}{c^2} \epsilon_2 \quad (2.39)$$

using Eq. 2.37 in 2.39 we get  $q_1^2 = -\epsilon_1^2 \frac{\omega^2}{c^2} \frac{1}{\epsilon_1 + \epsilon_2}$ . Plugging this last result into 2.38 and solving in region 1, we finally get the dispersion relation for a SP:

$$k(\omega) = \frac{\omega}{c} \sqrt{\frac{\epsilon_1 \epsilon_2}{\epsilon_1 + \epsilon_2}} \quad (2.40)$$

For the specific case of an interface between a metal and the vacuum (in which we will mainly be interested) Eq. 2.40 becomes:

$$k(\omega) = \frac{\omega}{c} \sqrt{\frac{1 - \omega_p^2/\omega^2}{2 - \omega_p^2/\omega^2}} \quad (2.41)$$

Figure 2.8 shows the propagation of a SP. The upper material is the dielectric, while the lower material is a metal. It is worth to remark that the electromagnetic field extends very little into the metal. In fact, the decay length is essentially the electron skin depth in this case.

The dispersion relation of Eq. 2.41 has an evident singularity when  $\omega \rightarrow \omega_p/\sqrt{2}$ . Then there's a gap for  $\omega_p/\sqrt{2} < \omega < \omega_p$  where  $k(\omega)$  is imaginary and finally there's



another branch of the dispersion function for  $\omega > \omega_p$ . For SPs only the lower branch is of interest ( $\omega < \omega_p/\sqrt{2}$ ), since the upper branch describes the propagation of very high frequency EM waves in the metal.

The previous derivation was performed for a metal. However it is valid also for a cold plasma, provided that relativistic effects are disregarded.

When  $\omega < \omega_p/\sqrt{2}$ ,  $k(\omega) > \omega/c$ . This implies that coupling between an EM wave in vacuum and a SP is impossible. In fact, the matching condition for an EM wave with an angle of incidence  $\theta$  reads as follow:

$$k_{EM}(\omega) \sin(\theta) = k_{SP}(\omega) \longrightarrow \frac{\omega}{c} \sin(\theta) = k_{SP}(\omega) \quad (2.42)$$

Equation 2.42 cannot be satisfied if  $\omega < \omega_p$  (in the previous equation  $k_{EM}$  and  $k_{SP}$  are, respectively, the  $k$  vector for the EM wave and the SP).

In general, the excitation of a surface plasmon by direct illumination of a flat interface can be proven to be impossible. Thus several schemes have been developed in order to excite a SP with an electromagnetic wave.<sup>15</sup> In the so-called *Otto* configuration, a dielectric prism is in direct contact with a metal thin surface. When an EM field is reflected at the dielectric-metal interface, its evanescent field component is responsible for the excitation of a surface plasmon on the back side of the metal thin foil. *Kretschmann* configuration is a very similar scheme, but in this case the aforementioned components are arranged in such a way to introduce a thin air gap between the prism and the metal. In this case the SP is excited by the evanescent EM field on the face of the metal foil facing the prism. These strategies are crucially based on the use of a dielectric.

The aforementioned schemes are clearly unsuitable for the aim of extending the study of plasmonics effects in high intensity laser-matter interaction. Indeed during the interaction with a high intensity laser pulse any dielectric becomes a strongly conductive plasma. Therefore, we must rely on other common schemes in “traditional” plasmonics involving a structuring of a metal interface. Among these techniques a widely used scheme consists in using metal surfaces with a shallow modulation of period  $d$  (if the modulation of the surface is not shallow, the dispersion relation of the SP can be strongly affected). The SP dispersion relation is then folded with period  $q = 2\pi/d$  in the  $k - \omega$  plane and the matching condition hence reads:

---

<sup>15</sup>Without using an EM wave, a SP can be excited also with accelerated charged particles.

$$K_{EM}(\omega) \sin(\theta) = k_{SP}(\omega) \pm n \frac{2\pi}{d} \quad (2.43)$$

where  $d$  is the groove spacing and  $n$  is an integer number.

A solution for the matching condition of Eq. 2.43 can then be found. For a given value of  $\omega$ , the condition of Eq. 2.43 depends only on the period of the grating  $d$  and the angle of incidence of the EM wave  $\phi_i$ :

$$\pm n \lambda_L / d = \sqrt{(1 - \omega_p^2 / \omega^2) / (2 - \omega_p^2 / \omega^2)} - \sin(\phi_i). \quad (2.44)$$

For a strongly over-dense plasma ( $\omega_p \gg \omega$ ), if we restrict to the solution with  $n = +1$ , the conditions for  $d$  and  $\phi_i$  becomes:

$$\frac{\lambda_L}{d} = 1 - \sin(\phi_i). \quad (2.45)$$

The matching condition is represented graphically in Fig. 2.9. Equation 2.45 is plotted in Fig. 2.10. Some selected values are highlighted.

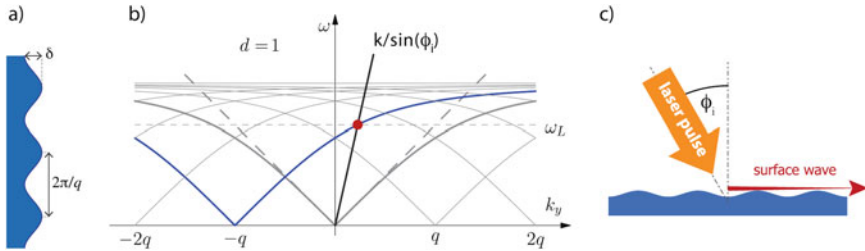


**Fig. 2.9** Pictorial representation of the excitation of a SP by a plane wave shining on a metal interface. The figure is reproduced with permission from [89]

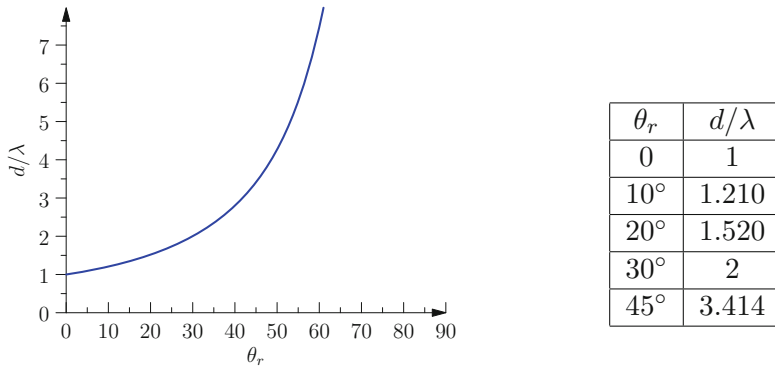


**Fig. 2.10** Relation between grating resonance angle and groove spacing  $d$

The theory presented so far is valid for non-relativistic laser-plasma interaction. It is important to stress that we are mainly interested in the extension of Plasmonics in the High Field regime, where we expect relativistic effects to be strong. Thus there's no "a priori" guarantee that the theory which we've exposed will hold at relativistic intensities. Indeed, a complete and convincing theory for surface plasmon polaritons in the relativistic regime (High Field Plasmonics) is still lacking in the literature.

### 2.3.2 Overview of Plasmonic Schemes and Applications

The impressive development of plasmonics in the last decades has led to the realization of a large amount of interesting schemes. Figure 2.11 gives an idea of the variety of Plasmonics schemes and its applications.

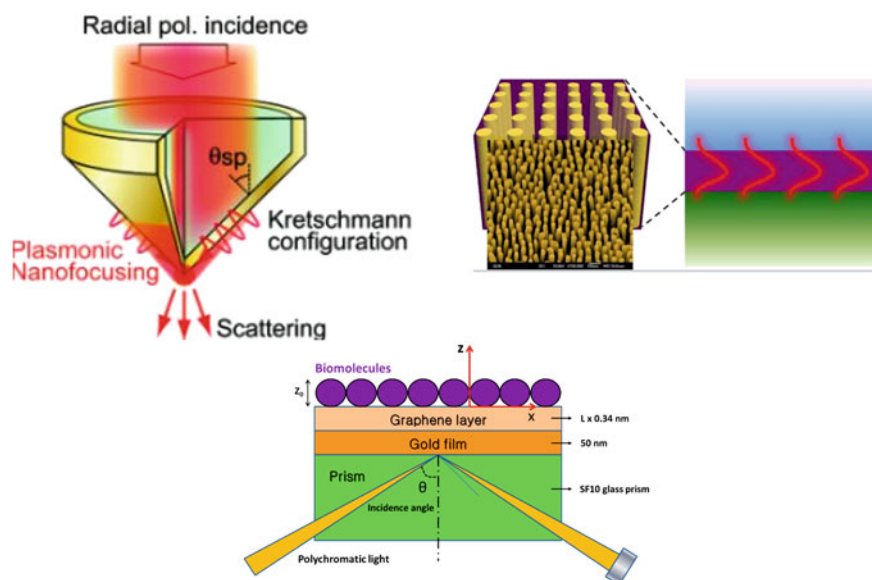


**Fig. 2.11** A few selected applications of plasmonics, which illustrate the variety of the field. Picture 1 shows a nanofocusing device, picture 2 shows a plasmonic metamaterial made of metallic nanorods, picture 3 shows the use of a plasmonic device for biosensing: the high field confinement achieved in plasmonic schemes is exploited to enhance biomolecules detection. Picture 1 is reproduced from Ono et al. Surface Plasmon Excitation and Localization by Metal-Coated Axicon Prism. *Micromachines*, 3 (2012) [90]. Copyright 2012 by the authors, released under a CC-BY license <http://creativecommons.org/licenses/by/3.0/>. Picture 2 is reproduced from Vasilantonakis et al. *Laser & Photonics Reviews*, 9 (2015) [91]. Copyright 2015 by the authors, released under a CC-BY license <http://creativecommons.org/licenses/by/3.0/>. Picture 3 is reproduced from Nguyen et al. Surface plasmon resonance: a versatile technique for biosensor applications. *Sensors*, 15 (2015) [92]. Copyright by the authors, released under a Creative Commons attribution license <http://creativecommons.org/licenses/by/4.0/>

In the the left upper panel, a device conceived to achieve plasmonic nanofocusing is shown. While propagating EM waves cannot be focused below the diffraction limit  $\lambda/2$ , surface plasmons are evanescent modes and can be concentrated much further. A variety of devices able to concentrate surface plasmons in structures much smaller than the wavelength of the exciting EM have been developed [93] (nanotips, tapered waveguides, kissing cylinders ...) leading to extreme field enhancements.<sup>16</sup> Plasmonic nanofocusing in metallic tips is currently exploited for technological applications such as the Scanning Near-field Optical Microscopy (SNOM) technique [94].

Plasmonic metamaterials [95] (see the top right panel of Fig. 2.11) are materials structured on a sub-wavelength scale which exploits plasmonics effects to achieve peculiar optical properties, which are not found in conventional materials. For instance, a plasmonic metamaterial may behave as a negative refraction index material. Suitably prepared plasmonics meta-surfaces may show unconventional optical properties as well (see [96]).

Plasmonic elements can be integrated into microfluidic lab-on-chips. The replacement of traditional electronic components with plasmonics equivalents is also an active research field [85].

An important technological application of SP is represented by biosensors (see [97]): a surface plasmon is excited on a suitably coated surface and the analysis of the reflected light can be used to gather information on the adsorbed molecules. The bottom panel of Fig. 2.11 provides a schematic of this technique.

Finally, the light trapping properties of SPs have been exploited to enhance the efficiency of solar cells [98].

Provided that plasmonics can be extended into the relativistic regime, the large variety of schemes already developed in traditional plasmonics could represent an interesting source of inspiration.

### 2.3.3 Outlook for Relativistic Plasmonics

The perspective of extending some schemes borrowed from classical plasmonics into the high field regime is certainly interesting. For instance, energy concentration schemes are particularly attractive, since they may lead to extreme laser intensities, currently out of reach for modern laser systems. Moreover, fine manipulation of ultra-high fields with structured targets may open the way for interesting possibilities.

Though potentially far-reaching, the advent of High Field Plasmonics could be hindered by fundamental difficulties inherent to high intensity laser-matter interaction. Indeed, several plasmonics schemes require sub-wavelength structuring of the targets: shallow gratings are required for laser coupling to surface plasmons, sub-wavelength tapered waveguides (or similar subwavelength structures) are required for light concentration beyond diffraction limit, subwavelength holes are required for plasmonic transparency schemes... However, in laser-matter interaction at relativistic

---

<sup>16</sup>Field enhancement exceeding  $100\times$  are reported in the literature.

intensities, electrons reach almost the speed of light in one laser cycle. This means that they can be displaced by  $\approx \lambda_{\text{Laser}}$  in a single laser cycle, which raises the concern that the subwavelength structures may not survive long enough.

Despite this issue, a few promising experimental results have been obtained recently with grating targets irradiated at relativistic intensities (see Chap. 4 for an extensive treatment). For instance, in a first experimental campaign in 2012 at CEA-Saclay, grating targets were irradiated with intense ( $I > 10^{19} \text{ W/cm}^2$ ) laser pulses at the resonant angle for SP excitation. This configuration was proven to enhance the cut-off energy of protons accelerated from the rear surface of the target [99]. A second experimental campaign was performed at the same facility in 2014 [100, 101]; the activity was focused on the effects of SP excitation on electron emission from grating targets. A strong emission of multi-MeV electron bunches was observed along the target surface only when a grating target was irradiated with an angle close to the one expected for the resonant SP excitation. Especially this second experimental campaign provides compelling evidence of SP excitation (a theoretical model together with 3D numerical simulations confirm that SP are involved in the electron acceleration process). These scheme represents a potentially attractive electron source for a few applications (see Chap. 4).

In addition, plasmonics effects can be identified in the Light Sail regime of Radiation pressure ion acceleration scheme (see Chap. 6 for a detailed discussion). Experimental evidence of complex structures in RPA ions was found in a few experiments [102], suggesting that the RPA scenario is prone to surface rippling instabilities, and structures closely resembling those determined by Rayleigh Taylor Instability were observed in several numerical studies. However, the scalelength of the structures observed in the simulations (close to the laser wavelength) cannot be explained with classical Rayleigh Taylor Instability theory. It is possible to show (both theoretically and numerically) that the plasmonic resonant coupling of the laser light with the target rippling affects the growth of RTI driven by the radiation pressure, determining the scale of the target rippling. These results are of interest because target rippling is possibly detrimental for the RPA scheme (since it may lead to an early onset of transparency).

In conclusion, though probably not all the schemes from traditional plasmonics can be easily ported into the high field regime, experimental and numerical evidence strongly supports SP excitation in relativistic laser-matter interaction. Besides their specific interest, these results open the way for further developments and support High Field Plasmonics as an emerging field in ultra-high intensity laser-matter interaction.

## References

1. J.P. Gordon, H.J. Zeiger, C.H. Townes, The maser new type of microwave amplifier, frequency standard, and spectrometer. *Phys. Rev.* **99**, 1264–1274 (1955)
2. O. Svelto, D.C. Hanna, *Principles of Lasers* (Springer, Berlin, 2009)
3. T.H. Maiman, Stimulated optical radiation in ruby. *Nature* **187**, 493–494 (1960)
4. (editorial). Fifty brilliant years. *Nat. Mater.* (2010)

5. V. Yanovsky, V. Chvykov, G. Kalinchenko, P. Rousseau, T. Planchon, T. Matsuoka, A. Maksimchuk, J. Nees, G. Cheriaux, G. Mourou, K. Krushelnick, Ultra-high intensity- 300-TW laser at 0.1 Hz repetition rate. *Opt. Express* **16**(3), 2109–2114 (2008)
6. Wikipedia (picture released as “public domain”). History of laser intensity (2007); (online). Accessed 01 May 2016
7. F.J. McClung, R.W. Hellwarth, Giant optical pulsations from ruby. *J. Appl. Phys.* **33**(3), 828–829 (1962)
8. A.H. Haus, Mode-locking of lasers. *IEEE J. Sel. Top. Quantum Electron.* **6**(6), 1173–1185 (2000)
9. International Energy Agency (ed.), *Key World Energy Statistics* (IEA, 2014)
10. J.E. Geusic, H.M. Marcos, L.G. Van Uitert, Laser oscillations in Nd-doped yttrium aluminium, yttrium gallium and gadolinium garnets. *Appl. Phys. Lett.* **4**(10), 182 (1964)
11. C.K.N. Patel, Continuous-wave laser action on vibrational-rotational transitions of CO<sub>2</sub>. *Phys. Rev.* **136**, A1187–A1193 (1964)
12. I.V. Pogorelsky, I. Ben-Zvi, J. Skaritka, M. Babzien, M.N. Polyanskiy, Z. Najmudin, N. Dover, W. Lu, New opportunities for strong-field LPI research in the mid-IR. *Proc. SPIE* **9509**, 95090P–95090P-10 (2015)
13. M.N. Polyanskiy, M. Babzien, I. Pogorelsky, V. Yakimenko. Ultrashort-pulse CO<sub>2</sub> lasers: ready for the race to petawatt? *Proc. SPIE* **8677**, 86770G–86770G-6 (2013)
14. D. Strickland, G. Mourou, Compression of amplified chirped optical pulses. *Opt. Commun.* **55**(6), 447–449 (1985)
15. Wikipedia (figure released as “public domain”). Chirped pulse amplification (2006); (online). Accessed 01 May 2016
16. B. Dromey, S. Kar, M. Zepf, P. Foster, The plasma mirror - a subpicosecond optical switch for ultrahigh power lasers. *Rev. Sci. Instrum.* **75**(3), 645–649 (2004)
17. C. Thaury, F. Quéré, J.-P. Geindre, A. Levy, T. Ceccotti, P. Monot, M. Bougeard, F. Reau, P. d’Oliveira, P. Audebert, R. Marjoribanks, Ph. Martin, Plasma mirrors for ultrahigh-intensity optics. *Nat. Phys.* **3**, 424–429 (2007)
18. C. Danson, D. Hillier, N. Hopps, D. Neely, Petawatt class lasers worldwide. *High Power Laser Sci. Eng.* **3** (2015)
19. I.W. Choi, Upgrade to 4 PW of the PULSER laser system, CoReLS, Institute for Basic Science, GIST, Gwangju, South Korea. personal communication
20. G. Chériaux, F. Giambruno, A. Frénaux, F. Leconte, L.P. Ramirez, P. Georges, F. Druon, D.N. Papadopoulos, A. Pellegrina, C. Le Blanc, I. Doyen, L. Legat, J.M. Boudenne, G. Mennerat, P. Audebert, G. Mourou, F. Mathieu, J.P. Chambaret, Apollon-10P: status and implementation. *AIP Conf. Proc.* **1462**(1), 78–83 (2012)
21. C. Hernandez-Gomez, S.P. Blake, O. Chekhlov, R.J. Clarke, A.M. Dunne, M. Galimberti, S. Hancock, R. Heathcote, P. Holligan, A. Lyachev, P. Matousek, I.O. Musgrave, D. Neely, P.A. Norreys, I. Ross, Y. Tang, T.B. Winstone, B.E. Wyborn, J. Collier, The Vulcan 10 PW project. *J. Phys.: Conf. Ser.* **244**(3), 032006 (2010)
22. A. Dubietis, G. Jonušauskas, A. Piskarskas, Powerful femtosecond pulse generation by chirped and stretched pulse parametric amplification in BBO crystal. *Opt. Commun.* **88**(4–6), 437–440 (1992)
23. I.N. Ross, P. Matousek, M. Towrie, A.J. Langley, J.L. Collier, The prospects for ultrashort pulse duration and ultrahigh intensity using optical parametric chirped pulse amplifiers. *Opt. Commun.* **144**(1–3), 125–133 (1997)
24. I.N. Ross, P. Matousek, G.H.C. New, K. Osvay, Analysis and optimization of optical parametric chirped pulse amplification. *J. Opt. Soc. Am. B* **19**(12), 2945–2956 (2002)
25. X. Liang, L. Yu, L. Xu, Y. Chu, Y. Xu, C. Wang, X. Lu, Y. Leng, R. Li, Z. Xu. Latest progress and research status of ultra-high intensity lasers at siom, in *Advanced Solid State Lasers* (Optical Society of America, 2014), p. AM1A.1
26. T. Ebisuzaki, M.N. Quinn, S. Wada, L.W. Piotrowski, Y. Takizawa, M. Casolino, M.E. Bertaina, P. Gorodetzky, E. Parizot, T. Tajima, R. Souillard, G. Mourou, Demonstration designs for the remediation of space debris from the international space station. *Acta Astronaut.* **112**, 102–113 (2015)

27. V.Yu. Bychenkov, A.V. Brantov, G. Mourou, Tc-99m production with ultrashort intense laser pulses. *Laser Particle Beams* **32**, 605–611 (2014)
28. M. Gerard, B. Brocklesby, T. Tajima, J.J. Limpert, The future is fibre accelerators. *Nat. Photonics* **7**, 258–261 (2013)
29. C. Labaune, D. Hulin, A. Galvanauskas, G.A. Mourou, On the feasibility of a fiber-based inertial fusion laser driver. *Opt. Commun.* **281**(15–16), 4075–4080 (2008)
30. P. Gibbon, *Short Pulse Laser Interactions with Matter* (Imperial College Press, London, 2005)
31. A. Macchi, *A Superintense Laser-Plasma Interaction Theory Primer* (Springer, Netherlands, 2013)
32. P. Mulser, D. Bauer, *High Power Laser-Matter Interaction*, vol. 238 (Springer, Berlin, 2010)
33. S.R. Groot, W.A. Leeuwen, C.G. van Weert, *Relativistic Kinetic Theory: Principles and Applications* (North-Holland, Amsterdam, 1980)
34. A.W. Trivelpiece, N.A. Krall, *Principles of Plasma Physics* (McGraw-Hill, Englewood Cliffs, 1973)
35. J.D. Jackson, J.D. Jackson, *Classical Electrodynamics*, vol. 3 (Wiley, New York, 1962)
36. A. Macchi, M. Borghesi, M. Passoni, Ion acceleration by superintense laser-plasma interaction. *Rev. Mod. Phys.* **85**, 751–793 (2013)
37. F. Brunel, Anomalous absorption of high intensity subpicosecond laser pulses. *Phys. Fluids* (1958–1988) **31**(9), 2714–2719 (1988)
38. H. Popescu, S.D. Baton, F. Amiranoff, C. Rousseaux, M. Rabec Le Gloahec, J.J. Santos, L. Gremillet, M. Koenig, E. Martinolli, T. Hall, J.C. Adam, A. Heron, D. Batani, Subfemtosecond, coherent, relativistic, and ballistic electron bunches generated at  $\omega_0$  and  $2\omega_0$  in high intensity laser-matter interaction. *Phys. Plasmas* **12**(6), 063106 (2005)
39. P. Mulser, H. Ruhl, J. Steinmetz, Routes to irreversibility in collective laser-matter interaction. *Laser Particle Beams* **19**, 23–28 (2001)
40. W.L. Kruer, K. Estabrook, J $\times$ B heating by very intense laser light. *Phys. Fluids* **28**(1), 430–432 (1985)
41. C. Perego, A. Zani, D. Batani, M. Passoni, Extensive comparison among target normal sheath acceleration theoretical models. *Nucl. Instrum. Methods Phys. Res. Sect. A: Accel. Spectrom. Detect. Assoc. Equip.* **653**(1), 89–93 (2011); Superstrong 2010
42. M. Lontano, M. Passoni, Electrostatic field distribution at the sharp interface between high density matter and vacuum. *Phys. Plasmas* **13**(4), 042102 (2006)
43. L.D. Landau, E.M. Lifshitz, *Course of Theoretical Physics Series (Book 2)*, vol. 2 (*The Classical Theory of Fields*), chapter 76 (Butterworth-Heinemann, London, 1980)
44. M. Tamburini, F. Pegoraro, A. Di Piazza, C.H. Keitel, A. Macchi, Radiation reaction effects on radiation pressure acceleration. *New J. Phys.* **12**(12), 123005 (2010)
45. A. Di Piazza, Exact solution of the Landau-Lifshitz equation in a plane wave. *Lett. Math. Phys.* **83**(3), 305–313 (2008)
46. A. Di Piazza, K.Z. Hatsagortsyan, C.H. Keitel, Quantum radiation reaction effects in multiphoton Compton scattering. *Phys. Rev. Lett.* **105**, 220403 (2010)
47. T. Tajima, J.M. Dawson, Laser electron accelerator. *Phys. Rev. Lett.* **43**, 267–270 (1979)
48. J. Faure, Y. Glinec, A. Pukhov, S. Kiselev, S. Gordienko, E. Lefebvre, J.-P. Rousseau, F. Burgy, V. Malka, A laser-plasma accelerator producing monoenergetic electron beams. *Nature* **431**, 541–544 (2004)
49. W.P. Leemans, A.J. Gonsalves, H.-S. Mao, K. Nakamura, C. Benedetti, C.B. Schroeder, Cs. Tóth, J. Daniels, D.E. Mittelberger, S.S. Bulanov, J.-L. Vay, C.G.R. Geddes, E. Esarey, Multi-GeV electron beams from capillary-discharge-guided subpetawatt laser pulses in the self-trapping regime. *Phys. Rev. Lett.* **113**, 245002 (2014)
50. H.T. Kim, K.H. Pae, H.J. Cha, I.J. Kim, T.J. Yu, J.H. Sung, S.K. Lee, T.M. Jeong, J. Lee, Enhancement of electron energy to the multi-GeV regime by a dual-stage laser-wakefield accelerator pumped by petawatt laser pulses. *Phys. Rev. Lett.* **111**, 165002 (2013)
51. C. Benedetti, C.B. Schroeder, E. Esarey, W.P. Leemans, Plasma wakefields driven by an incoherent combination of laser pulses: a path towards high-average power laser-plasma accelerators. *Phys. Plasmas* **21**(5), 056706 (2014)



52. S. Corde, E. Adli, J.M. Allen, W. An, C.I. Clarke, C.E. Clayton, J.P. Delahaye, J. Frederico, S. Gessner, S.Z. Green, M.J. Hogan, C. Joshi, N. Lipkowitz, M. Litos, W. Lu, K.A. Marsh, W.B. Mori, M. Schmeltz, N. Vafaei-Najafabadi, D. Walz, V. Yakimenko, G. Yocky, Multi-gigaelectronvolt acceleration of positrons in a self-loaded plasma wakefield. *Nature* **524**, 442–445 (2015)
53. H. Daido, M. Nishiuchi, A.S. Pirozhkov, Review of laser-driven ion sources and their applications. *Rep. Prog. Phys.* **75**(5), 056401 (2012)
54. M. Lewenstein, Ph Balcou, MYu. Ivanov, A. L'Huillier, P.B. Corkum, Theory of high-harmonic generation by low-frequency laser fields. *Phys. Rev. A* **49**, 2117–2132 (1994)
55. P.B. Corkum, Plasma perspective on strong field multiphoton ionization. *Phys. Rev. Lett.* **71**, 1994–1997 (1993)
56. G. Sansone, E. Benedetti, F. Calegari, C. Vozzi, L. Avaldi, R. Flammini, L. Poletto, P. Villoresi, C. Altucci, R. Velotta, S. Stagira, S. De Silvestri, M. Nisoli, Isolated single-cycle attosecond pulses. *Science* **314**(5798), 443–446 (2006)
57. E.J. Takahashi, P. Lan, T. Okino, Y. Furukawa, Y. Nabekawa, K. Yamanouchi, K. Midorikawa, Intense attosecond pulses for probing ultrafast molecular dynamics, in *Ultrafast Phenomena XIX, vol. 162 of Springer Proceedings in Physics*, ed. by K. Yamanouchi, S. Cundiff, R. de Vivie-Riedle, M. Kuwata-Gonokami, L. DiMauro (Springer, Berlin, 2015), pp. 16–19
58. U. Teubner, P. Gibbon, High-order harmonics from laser-irradiated plasma surfaces. *Rev. Mod. Phys.* **81**, 445–479 (2009)
59. F. Quéré, C. Thaury, P. Monot, S. Dobosz, J.-P. Ph Martin, P. Audebert, Geindre, Coherent wake emission of high-order harmonics from overdense plasmas. *Phys. Rev. Lett.* **96**, 125004 (2006)
60. S. Corde, K. Ta, Phuoc, G. Lambert, R. Fitour, V. Malka, A. Rousse, A. Beck, E. Lefebvre, Femtosecond x rays from laser-plasma accelerators. *Rev. Mod. Phys.* **85**, 1–48 (2013)
61. G. Sarri, D.J. Corvan, W. Schumaker, J.M. Cole, A. Di Piazza, H. Ahmed, C. Harvey, C.H. Keitel, K. Krushelnick, S.P.D. Mangles, Z. Najmudin, D. Symes, A.G.R. Thomas, M. Yeung, Z. Zhao, M. Zepf, Ultrahigh brilliance multi-MeV  $\gamma$ -ray beams from nonlinear relativistic Thomson scattering. *Phys. Rev. Lett.* **113**, 224801 (2014)
62. H.W. Koch, J.W. Motz, Bremsstrahlung cross-section formulas and related data. *Rev. Mod. Phys.* **31**, 920–955 (1959)
63. H. Schwoerer, P. Gibbon, S. Düsterer, R. Behrens, C. Ziener, C. Reich, R. Sauerbrey, MeV x-rays and photoneutrons from femtosecond laser-produced plasmas. *Phys. Rev. Lett.* **86**, 2317–2320 (2001)
64. I. Pomerantz, E. McCary, A.R. Meadows, A. Arefiev, A.C. Bernstein, C. Chester, J. Cortez, M.E. Donovan, G. Dyer, E.W. Gaul, D. Hamilton, D. Kuk, A.C. Lestrade, C. Wang, T. Ditmire, B.M. Hegelich, Ultrashort pulsed neutron source. *Phys. Rev. Lett.* **113**, 184801 (2014)
65. Y. Arikawa, M. Utsugi, A. Morace, T. Nagai, Y. Abe, S. Kojima, S. Sakata, H. Inoue, S. Fujioka, Z. Zhang, H. Chen, J. Park, J. Williams, T. Morita, Y. Sakawa, Y. Nakata, J. Kawanaka, T. Jitsuno, N. Sarukura, N. Miyana, H. Azechi, High-intensity neutron generation via laser-driven photonuclear reaction. *Plasma Fusion Res.* **10**, 2404003 (2015)
66. M. Roth, D. Jung, K. Falk, N. Guler, O. Deppert, M. Devlin, A. Favalli, J. Fernandez, D. Gautier, M. Geissel, R. Haight, C.E. Hamilton, B.M. Hegelich, R.P. Johnson, F. Merrill, G. Schaumann, K. Schoenberg, M. Schollmeier, T. Shimada, T. Taddeucci, J.L. Tybo, F. Wagner, S.A. Wender, C.H. Wilde, G.A. Wurden, Bright laser-driven neutron source based on the relativistic transparency of solids. *Phys. Rev. Lett.* **110**, 044802 (2013)
67. C. Gongyin, R.C. Lanza, Fast neutron resonance radiography for elemental imaging: theory and applications. *IEEE Trans. Nucl. Sci.* **49**(4), 1919–1924 (2002)
68. C.L. Fink, B.J. Micklich, T.J. Yule, P. Humm, L. Sagalovsky, M.M. Martin, Evaluation of neutron techniques for illicit substance detection. *Nucl. Instrum. Methods Phys. Res. Sect. B: Beam Interact. Mater. Atoms* **99**(1–4), 748–752 (1995); Application of Accelerators in Research and Industry'94
69. J. Rynes, J. Bendahan, T. Gozani, R. Loveman, J. Stevenson, C. Bell, Gamma-ray and neutron radiography as part of a pulsed fast neutron analysis inspection system. *Nucl. Instrum.*



- Methods Phys. Res. Sect. A: Accel. Spectrom. Detect. Assoc. Equip. **422**(1–3), 895–899 (1999)
70. J.C. Overley, M.S. Chmelik, R.J. Rasmussen, R.M.S. Schofield, H.W. Lefevre, Explosives detection through fast-neutron time-of-flight attenuation measurements. Nucl. Instrum. Methods Phys. Res. Sect. B: Beam Interact. Mater. Atoms **99**(1–4), 728–732 (1995). Application of Accelerators in Research and Industry'94
  71. J.E. Eberhardt, S. Rainey, R.J. Stevens, B.D. Sowerby, J.R. Tickner, Fast neutron radiography scanner for the detection of contraband in air cargo containers. Appl. Radiat. Isot. **63**(2), 179–188 (2005)
  72. C. Freiburghaus, S. Rosswog, F.-K. Thielemann, r-process in neutron star mergers. Astrophys. J. Lett. **525**(2), L121 (1999)
  73. S. Bouquet, E. Falize, C. Michaut, C.D. Gregory, B. Loupiau, T. Vinci, M. Koenig, From lasers to the universe: scaling laws in laboratory astrophysics. High Energy Density Phys. **6**(4), 368–380 (2010)
  74. É. Falize, A. Ravasio, B. Loupiau, A. Dizièrre, C.D. Gregory, C. Michaut, C. Busschaert, C. Cavet, M. Koenig, High-energy density laboratory astrophysics studies of accretion shocks in magnetic cataclysmic variables. High Energy Density Phys. **8**(1), 1–4 (2012). cited By 7
  75. G. Sarri, K. Poder, J.M. Cole, W. Schumaker, A. Di Piazza, B. Reville, T. Dzelzainis, D. Doria, L.A. Gizzi, G. Grittani, S. Kar, C.H. Keitel, K. Krushelnick, S. Kuschel, S.P.D. Mangles, Z. Najmudin, N. Shukla, L.O. Silva, D. Symes, A.G.R. Thomas, M. Vargas, J. Vieira, M. Zepf, Generation of neutral and high-density electron–positron pair plasmas in the laboratory. Nat. Commun. **6**, 6747 (2015)
  76. H. Chen, F. Fiuza, A. Link, A. Hazi, M. Hill, D. Hoarty, S. James, S. Kerr, D.D. Meyerhofer, J. Myatt, J. Park, Y. Sentoku, G.J. Williams, Scaling the yield of laser-driven electron-positron jets to laboratory astrophysical applications. Phys. Rev. Lett. **114**, 215001 (2015)
  77. D. Batani, A. Morelli, M. Tomasini, A. Benuzzi-Mounaix, F. Philippe, M. Koenig, B. Marchet, I. Masclet, M. Rabec, Ch. Reverdin, R. Cauble, P. Celliers, G. Collins, L. Da Silva, T. Hall, M. Moret, B. Sacchi, P. Baclet, B. Cathala, Equation of state data for iron at pressures beyond 10 Mbar. Phys. Rev. Lett. **88**, 235502 (2002)
  78. A.L. Kitcher, T. Döppner, D. Swift, J. Hawreliak, G. Collins, J. Nilsen, B. Bachmann, E. Dewald, D. Strozzi, S. Felker, O.L. Landen, O. Jones, C. Thomas, J. Hammer, C. Keane, H.J. Lee, S.H. Glenzer, S. Rothman, D. Chapman, D. Kraus, P. Neumayer, R.W. Falcone, Probing matter at Gbar pressures at the NIF. High Energy Density Phys. **10**, 27–34 (2014)
  79. M.A. Purvis, V.N. Shlyaptsev, R. Hollinger, C. Bargsten, A. Pukhov, A. Prieto, Y. Wang, B.M. Luther, L. Yin, S. Wang, J.J. Rocca, Relativistic plasma nanophotonics for ultrahigh energy density physics. Nat. Photonics **7**, 796–800 (2013)
  80. A. Di Piazza, C. Müller, K.Z. Hatsagortsyan, C.H. Keitel, Extremely high-intensity laser interactions with fundamental quantum systems. Rev. Mod. Phys. **84**, 1177–1228 (2012)
  81. Surface plasmon resurrection (editorial). Nat. Photonics **6**, 707 (2012)
  82. W.L. Barnes, A. Dereux, T.W. Ebbesen, Surface plasmon subwavelength optics. Nature **424**(6950), 824–830 (2003)
  83. D.K. Gramotnev, S.I. Bozhevolnyi, Plasmonics beyond the diffraction limit. Nat. Photonics **4**, 83–91 (2010)
  84. A.G. Brolo, Plasmonics for future biosensors. Nat. Photonics **6**(11), 709–713 (2012)
  85. E. Ozbay, Plasmonics: merging photonics and electronics at nanoscale dimensions. Science **311**(5758), 189–193 (2006)
  86. V.A. Vshivkov, N.M. Naumova, F. Pegoraro, S.V. Bulanov, Nonlinear electrodynamics of the interaction of ultra-intense laser pulses with a thin foil. Phys. Plasmas **5**(7), 2727–2741 (1998)
  87. J.M. Pitarke, V.M. Silkin, E.V. Chulkov, P.M. Echenique, Theory of surface plasmons and surface-plasmon polaritons. Rep. Prog. Phys. **70**(1), 1 (2007)
  88. S.A. Maier, *Plasmonics: Fundamentals and Applications* (Springer, New York, 2007)
  89. A. Sgattoni, L. Fedeli, G. Cantono, T. Ceccotti, A. Macchi, High field plasmonics and laser-plasma acceleration in solid targets. Plasma Phys. Control. Fusion **58**(1), 014004 (2016)

90. A. Ono, H. Sano, W. Inami, Y. Kawata, Surface plasmon excitation and localization by metal-coated axicon prism. *Micromachines* **3**(1), 55 (2012)
91. N. Vasilantonakis, M.E. Nasir, W. Dickson, G.A. Wurtz, A.V. Zayats, Bulk plasmon-polaritons in hyperbolic nanorod metamaterial waveguides. *Laser Photonics Rev.* **9**(3), 345–353 (2015)
92. H.H. Nguyen, J. Park, S. Kang, M. Kim, Surface plasmon resonance: a versatile technique for biosensor applications. *Sensors* **15**(5), 10481–10510 (2015)
93. D.K. Gramotnev, S.I. Bozhevolnyi, Nanofocusing of electromagnetic radiation. *Nat. Photonics* **8**, 13–22 (2014)
94. D.W. Pohl, U.Ch. Fischer, U.T. Dürig, Scanning near-field optical microscopy (SNOM). *J. Microsc.* **152**(3), 853–861 (1988)
95. C.M. Soukoulis, M. Wegener, Past achievements and future challenges in the development of three-dimensional photonic metamaterials. *Nat. Photonics* **5**, 523–530 (2011)
96. A.V. Kildishev, A. Boltasseva, V.M. Shalae, Planar photonics with metasurfaces. *Science* **339**(6125) (2013)
97. B. Liedberg, C. Nylander, I. Lunström, Surface plasmon resonance for gas detection and biosensing. *Sens. Actuators* **4**, 299–304 (1983)
98. S. Pillai, K.R. Catchpole, T. Trupke, M.A. Green, Surface plasmon enhanced silicon solar cells. *J. Appl. Phys.* **101**(9), 093105 (2007)
99. T. Ceccotti, V. Floquet, A. Sgattoni, A. Bigongiari, O. Klimo, M. Raynaud, C. Riconda, A. Heron, F. Baffigi, L. Labate, L.A. Gizzi, L. Vassura, J. Fuchs, M. Passoni, M. Květon, F. Novotny, M. Possolt, J. Prokūpek, J. Proška, J. Pšikal, L. Štolcová, A. Velyhan, M. Bougeard, P. D'Oliveira, O. Tcherbakoff, F. Réau, P. Martin, A. Macchi, Evidence of resonant surface-wave excitation in the relativistic regime through measurements of proton acceleration from grating targets. *Phys. Rev. Lett.* **111**, 185001 (2013)
100. L. Fedeli, A. Sgattoni, G. Cantono, I. Prencipe, M. Passoni, O. Klimo, J. Proska, A. Macchi, T. Ceccotti, Enhanced electron acceleration via ultra-intense laser interaction with structured targets. *Proc. SPIE* **9514**, 95140R–95140R-8 (2015)
101. L. Fedeli, A. Sgattoni, G. Cantono, D. Garzella, F. Réau, I. Prencipe, M. Passoni, M. Raynaud, M. Kveton, J. Proska, A. Macchi, T. Ceccotti. Electron acceleration by relativistic surface plasmons in laser-grating interaction. *Phys. Rev. Lett.* **116**, 015001 (2016)
102. B. Eliasson, Instability of a thin conducting foil accelerated by a finite wavelength intense laser. *New J. Phys.* **17**(3), 033026 (2015)

High Field Plasmonics

Fedeli, L.

2017, XIX, 180 p. 83 illus., 30 illus. in color., Hardcover

ISBN: 978-3-319-44289-1